Work Order No. 582-19-93346-05
Contract No. 582-19-90500
Tracking No. 2019-15
Task 6

Prepared for:

Texas Commission on Environmental Quality
12100 Park 35 Circle MC 164
Austin, TX 78753

Prepared by:

Ramboll US Corporation
7250 Redwood Blvd., Suite 105
Novato, California 94945

August 15, 2019

Development and Testing of a Hemispheric Comprehensive Air Quality Model with Extensions (CAMx) Application

PREPARED UNDER A CONTRACT FROM THE
TEXAS COMMISSION ON ENVIRONMENTAL QUALITY

The preparation of this document was financed through a contract from the State of Texas through the Texas Commission on Environmental Quality.
The content, findings, opinions and conclusions are the work of the author(s) and do not necessarily represent findings, opinions or conclusions of the TCEQ.

RAMBOLL

Development and Testing of a Hemispheric Comprehensive Air Quality Model with Extensions (CAMx) Application

Ramboll
7250 Redwood Boulevard
Suite 105
Novato, CA 94945
USA

T +1 415 899 0700
https://ramboll.com

Contents

Table of Figures

Table of Tables

List of Acronyms

2-D	Two dimensional
3-D	Three dimensional
BC	Boundary concentrations
BEIS	Biogenic Emissions Inventory System
BNDEXTR	Boundary extraction program for 1-way nesting applications
CAMx	Comprehensive Air quality Model with extensions
CB6r3/AE6	Carbon Bond 6 revision 3 with CMAQ Aerosol v6 chemistry mechanism
CB6r4/CF	Carbon Bond 6 revision 4 with CAMx Coarse/Fine aerosol chemistry mechanism
CEDS	Community Emissions Data System
CiG	Cloud-in-Grid sub-grid convection model
CMAQ	Community Multiscale Air Quality model
CMAQ2CAMx	CMAQ-to-CAMx translation program
CPU	Central Processing Unit
DMS	Dimethyl sulfide
EDGAR	Emission Database for Global Atmospheric Research
EMAC	Global chemistry-climate model
EPA	US Environmental Protection Agency
EQSAM	Equilibrium Simplified Aerosol Model
FINN	Fire Inventory from NCAR
GEIA	Global Emissions Initiative
GEOS-Chem	Goddard Earth Observing System global model with Chemistry
GEOS2AQM	GEOS-Chem to CAMx interface program
Gb	Gigabyte
GHz	Gigahertz
H-CAMx	Hemispheric CAMx
HTAP	Hemispheric Transport of Air Pollution
IC	Initial concentrations
ISORRIOPIA	Inorganic aerosol equilibrium partitioning model
km	kilometers
Kv	Vertical diffusivity
KVPATCH	Kv adjustment program
LNOx	Lightning NOx
m	meters
mb	millibars
MDA8	Maximum Daily 8-hour Average

MEGAN	Model of Emissions of Gases and Aerosols from Nature
MOPITT	Measurement of Pollution in the Troposphere
MPI	Message Passing Interface parallel processing
NASA	National Aeronautics and Space Administration
NCAR	National Center for Atmospheric Research
netCDF	Network Common Data Form
NOx	Nitrogen oxides (nitrogen oxide + nitrogen dioxide)
NOy	All oxidized nitrogen compounds including NOx
NRTEEM	Near Real Time Exceptional Event Modeling
O_3	Ozone
O3MAP	Column ozone mapping program
OCEANIC	Oceanic emissions program
OMI, AIRS	Ozone Monitoring Instrument
OMPS	Suomi-NPP Ozone Mapping and Profiler Suite
OMP	Open multi-processor parallelization
OSAT	Ozone Source Apportionment Technology
PM	Particulate matter
ppb	Parts per billion by volume
PS	Polar Stereographic
PSAT	Particulate Source Apportionment Technology
PV	Potential Vorticity
QAPP	Quality Assurance Project Plan
QA/QC	Quality Assurance / Quality Control
ROH	Rest of hemisphere
SA	Source Apportionment
SIP	State Implementation Plan
SO_2	Sulfate dioxide
STE	Stratospheric-Tropospheric Exchange
TCEQ	Texas Commission on Environmental Quality
TKE	Turbulent Kinetic Energy
TUV	Tropospheric Ultraviolet and Visible radiative transfer model
U/V	U-component (east-west) and V-component (north-south) wind speed
VOC	Volatile organic compounds
WBDUST	Wind-blown dust emissions program
WMO	World Meteorological Organization
WRAP	Western Regional Air Partnership
WRF	Weather and Research Forecasting model
WRFCAMx	WRF-to-CAMx interface program
YSU	Yonsei University boundary layer scheme

EXECUTIVE SUMMARY

This project successfully developed an application of the Comprehensive Air quality Model with Extensions (CAMx) covering the Northern Hemisphere for the May-September 2016 season. The hemispheric application, referred to as "H-CAMx", included an example source apportionment run for the month of September 2016. Ramboll developed a modeling protocol at the beginning of the project that established a plan to implement certain updates to the CAMx model to support hemispheric modeling; describes available sources of input data, pre-processing, and various data-model interface steps; and approaches for evaluating model output.

The TCEQ runs CAMx on regional-scale modeling grids to support regulatory assessments for ozone. TCEQ also uses the Goddard Earth Observing System model with Chemistry (GEOS-Chem), a global photochemical model, to develop initial/boundary concentrations for TCEQ's regional CAMx applications. GEOS-Chem uses different chemical mechanisms than CAMx, lacks a source apportionment capability, and its science updates are frequently out-of-step with the latest enhancements to CAMx. In FY-2018, Ramboll conducted a scoping study for TCEQ to assess the feasibility of applying CAMx over the Northern Hemisphere, finding that it is both feasible and desirable to pursue this goal. The advantages and tangible benefits of H-CAMx range from chemical consistency to seamless integration of the CAMx Source Apportionment (SA) tool, and to immediate availability of future CAMx updates and enhancements for both regional and hemispheric applications. H-CAMx will greatly improve TCEQ's ability to characterize the impact of global emissions on Texas air quality.

H-CAMx utilizes input data for 2016 (e.g., meteorology and emissions) prepared by the US Environmental Protection Agency (EPA) for hemispheric CMAQ. Ramboll developed additional ancillary input datasets specific to CAMx, including photolysis data, initial/boundary/top concentrations, and certain natural emission components such as oceanic sources (sea salt, iodine, sulfates) and wind-blown dust. The H-CAMx modeling domain is based on a polar stereographic projection with 187x187 grid cells, each 108 km in size, and 44 vertical layers spanning from the Earth's surface to roughly an altitude of 20 km. EPA generated meteorological inputs using the Weather Research and Forecasting meteorological model (WRF), which Ramboll processed through the WRFCAMx interface program. EPA's hemispheric emissions dataset included global anthropogenic emissions based on the 2010 Emission Database for Global Atmospheric Research (EDGAR) Hemispheric Transport of Air Pollution (HTAP), version 2, which were projected to 2014 using and the Community Emissions Data System (CEDS). Specific regional inventories were incorporated for the US, Canada, Mexico, and several inventories for Asia and China. Natural emissions include wildfire emissions from a combination of the Fire Inventory from NCAR (FINN) and the EPA's 2016 US emissions inventory; biogenic emissions from the Model of Emissions of Gases and Aerosols from Nature (MEGAN) and the EPA's US Biogenic Emissions Inventory System (BEIS); and lightning NOx from monthly estimates reported by the Global Emissions Initiative (GEIA). Ramboll converted these gridded and point source datasets to CAMx speciation and formats.

We elected to develop hemispheric initial/boundary/top concentrations from pre-existing global model output from our 2016 GEOS-Chem simulation, which provided several advantages over EPA's inputs, particularly in shortening the time for H-CAMx "spin-up" from initial concentrations and the ability to specify stratospheric ozone from top concentrations. We implemented a special modification to CAMx to include this stratospheric ozone treatment. It was also necessary to modify the CAMx Ozone Source Apportionment Technology (OSAT) to accommodate the new stratospheric ozone treatment. However, this method requires H-CAMx to rely on output from another global model to supply top boundary concentrations, so H-CAMx is not an entirely independent model.

We ran H-CAMx over May through September 2016, with a one-month spin-up period (April) from initial concentrations. Two initial runs were inert so that we could quickly review the evolution of ozone initial, boundary and top concentrations and the influence of our stratospheric ozone treatment. One inert run included the stratospheric ozone treatment described in Section 2, while the other did not so that ozone in the stratosphere evolved strictly via dispersion of initial/boundary/top concentrations. Differences between the two were reviewed via graphical animations and against global ozonesonde profile data to assess which was more appropriately characterizing stratospheric and upper tropospheric ozone profiles. The run with no stratospheric treatment greatly over predicted ozone globally, while the run with stratospheric treatment dramatically reduced the over prediction bias. Based on that analysis, we chose to continue using the stratospheric ozone treatment.

We then ran two full chemistry simulations and evaluated results against the same ozonesonde data. At the surface, the full chemistry runs generated much higher ozone than the inert run in Asia, middle east and Africa, while reducing ozone over the oceans substantially due to the marine chemical environment. In the mid-troposphere, ozone patterns were similar between the inert and full chemistry runs, except for somewhat higher ozone by roughly 10-40 ppb over the mid-latitudes, presumably due to chemical production from anthropogenic precursor emissions. Near the top of the model well into the stratosphere, results from inert and full chemistry runs were practically identical as we would expect. Overall, the full chemistry run resulted in a modest increase in the general over predictions seen in the inert results. We tested an alternative interpolation method for the stratospheric treatment, which exhibited much improved agreement with ozonesonde data in the troposphere, but at the expense of ozone under predictions in the stratosphere. Since it is more important to properly simulate the range of tropospheric ozone in H-CAMx for the purposes of supporting TCEQ regional modeling, the CAMx model code delivered to TCEQ for this project includes the alternative stratospheric treatment.

We included an application of OSAT to quantify foreign contributions to ozone concentrations in Texas ozone nonattainment areas. We configured OSAT to track emissions from six regions of the northern hemisphere: US, Canada, Mexico, Central and South America, Asia, and all others (rest of hemisphere, or ROH). OSAT tracked only a single emission sector (all anthropogenic and natural emissions). We ran H-CAMx/OSAT for the month of September 2016, including a 10-day spin up period from August 16, and generated time series of contributions to maximum daily 8-hour (MDA8) ozone from the six regions and initial/boundary concentrations in four Texas ozone nonattainment areas: Houston, Dallas, San Antonio and El Paso. In all cities except for El Paso, H-CAMx showed that US emissions are by far the dominant contributor, with large contributions from the ROH region (5-10 ppb) and occasional contributions from Mexico up to 5 ppb. In El Paso, H-CAMx estimated a larger mix of significant contributors including Mexico. Contributions from Canada, Asia and Latin America were negligible to small in all cases.

As part of this work, we expanded the CAMx SA tool to allow for 1-way nesting of SA tracers via initial/boundary concentrations. For example, a CAMx SA model application for the continental US can now read source apportioned boundary concentration (BC) files and track ozone and PM contributions from areas outside the continental US. The source apportioned BC files can be prepared from global model zero-out runs or an H-CAMx SA simulation. Alternatively, modeling for a US non-attainment area could obtain source apportioned BC files from a pre-existing continental-scale CAMx SA simulation. Details are given in Section 4. We have delivered new CAMx and IC/BC interface pre-processor code to TCEQ for additional testing and use. In Chapter 5 we recommend the several updates and additional analyses for future work.

1.0 INTRODUCTION

1.1 Background

The TCEQ uses the Comprehensive Air quality Model with Extensions (CAMx; Ramboll, 2018) for State Implementation Planning (SIP) purposes. CAMx requires input datasets that specify the temporal and spatial distributions of a multitude of chemical concentrations for initial and boundary concentrations (IC and BC). TCEQ uses a global chemical transport model called the Goddard Earth Observing System model with Chemistry (GEOS-Chem; Bey et al., 2001; Harvard, 2019) to develop CAMx IC/BC on a domain spanning much of North America. However, GEOS-Chem is primarily intended for studies of the global atmosphere and so uses different atmospheric chemical mechanisms than CAMx to simulate ozone and particulate matter (PM). Additionally, GEOS-Chem lacks a source apportionment capability for tracking ozone and PM contributions back to the source categories and regions where precursors were emitted. Finally, due to different priorities, GEOS-Chem's development and science updates are frequently out-of-step with the latest enhancements to CAMx.

In FY-2018, Ramboll conducted a scoping study for TCEQ to assess the feasibility of applying CAMx over the Northern Hemisphere (Emery et al., 2018). Those results showed that it is both feasible and desirable to pursue this goal. The advantages and tangible benefits of hemispheric CAMx include: (1) a source of chemically consistent BCs for TCEQ's regional modeling applications; (2) a seamless integration of the CAMx Source Apportionment (SA) tool to track contributions from foreign sources to ozone and PM in Texas and other states; (3) chemical and physical consistency between global and regional scales in a single model framework; and (4) immediate availability of future CAMx updates and enhancements for hemispheric applications without the need to implement them in other global models. Since TCEQ is familiar with CAMx and its SA features, the Hemispheric CAMx (H-CAMx) could be readily subsumed into TCEQ's set of modeling tools. Successful implementation of H-CAMx will greatly improve TCEQ's ability to characterize the impact of emissions outside the boundaries of the current modeling domain on Texas air quality.

1.2 Purpose and Objectives

This project developed an application of H-CAMx for the Northern Hemisphere, providing a consistent, stream-lined global-to-regional modeling system that includes important Probing Tools for the evaluation of international transport impacts. Ramboll developed a full-scale implementation of H-CAMx for the summer 2016 and demonstrated the use of SA to quantify foreign contributions to ozone concentrations in Texas ozone nonattainment areas.

Ramboll developed a modeling protocol at the beginning of the project (Emery and Yarwood. 2019) that established a plan to implement certain updates to the CAMx model to support hemispheric modeling; describes available sources of input data, pre-processing, and various data-model interface steps; and approaches for evaluating model output. We followed the modeling protocol as closely as possible in each step of the project; where deviations were necessary, we discussed alternatives with the TCEQ Project Manager. The selection of a specific modeling year and season was based on a pre-existing CMAQ global modeling dataset available from the US Environmental Protection Agency (EPA). The protocol was guided by EPA's final Modeling Guidance for ozone, $PM_{2.5}$ and visibility State Implementation Plans (EPA, 2018a) as well as EPA's Global-Scale Simulation Model Operational Evaluation Protocol (EPA, 2018b). The modeling protocol also incorporated necessary elements of a Quality Assurance Project Plan (QAPP), including audits of data quality and reporting of quality assurance results.

This final report documents the approach and results from the H-CAMx application. Section 2 describes the preparation of Base Model inputs and necessary CAMx modifications to support hemispheric applications. Section 3 presents results for the May-September 2016 modeling period. Section 4 presents an example run of H-CAMx with SA. Section 5 presents a summary and recommendations for future uses of H-CAMx and additional improvements.

2.0 BASE MODEL INPUTS AND CAMx MODIFICATIONS

Ramboll acquired the EPA's 2016 hemispheric emissions and meteorological modeling datasets and converted them to CAMx input formats. Ramboll also developed additional ancillary input datasets specific to CAMx using our suite of pre-processors (i.e., total ozone column, photolysis rates, IC/BCs, certain natural emission components). These activities adhered to the modeling protocol as closely as possible and included quality assurance / quality control (QA/QC) checks of the model input data. Ramboll also implemented certain code modifications in CAMx and some pre-processors necessary for hemispheric applications.

2.1 Grid Projection and Resolution

The H-CAMx modeling domain aligns exactly with EPA's hemispheric map projection and grid specifications (Figure 2-1; Mathur et al., 2017). The map projection is polar stereographic (PS), which is the only option available in both CAMx and the Weather Research and Forecasting meteorological model (WRF; Skamarock et al., 2008) that can include the North Pole without a mathematical singularity. The PS projection defines a secant latitude of 45°N where the map is "true"; this results in increasing spatial distortion away from this latitude toward the North Pole and the Equator. The "north-south" direction of the rectangular grid aligns along a "standard meridian" (98°W in this case). The domain comprises a square array of grid cells (187x187) with horizontal resolution of 108 km (~1°) centered on the North Pole. This resolution is better than most global models (e.g., 200-300 km or 2-3°) that are widely used to supply BCs to regional models. Further, this resolution has been found by Eastham and Jacob (2017) to be optimal in preserving intercontinental plume coherence according to their tests employing the standard vertical layer structure in the GEOS-Chem global chemistry model.

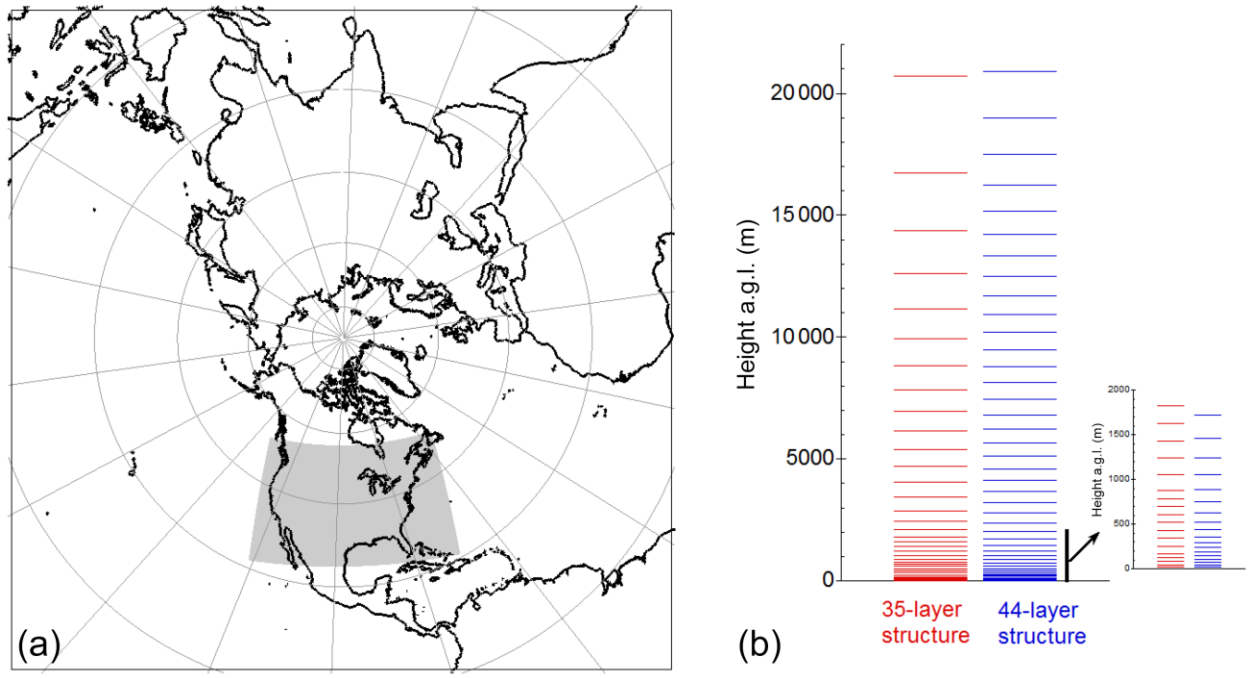

Figure 2-1. (a) EPA's hemispheric modeling domain on a polar stereographic projection with horizontal grid resolution of 108 km (the shaded region indicates a typical continental US grid). (b) Two vertical layer structures used by EPA for hemispheric applications. Figures taken from Mathur et al. (2017), Figure 2.

Table 2-1. The H-CAMx 44 vertical layer structure. Sigma refers to the normalized pressure coordinate used in WRF.

Layer Index	Layer Interface Height (m)	Layer Interface Sigma
1	21	0.998
2	45	0.995
3	73	0.991
4	105	0.988
5	142	0.983
6	185	0.978
7	234	0.972
8	290	0.966
9	357	0.958
10	433	0.949
11	521	0.939
12	623	0.928
13	742	0.914
14	881	0.899
15	1042	0.881
16	1230	0.861
17	1452	0.837
18	1712	0.810
19	2019	0.780
20	2385	0.744
21	2783	0.707
22	3198	0.669
23	3630	0.632
24	4083	0.595
25	4556	0.557
26	5054	0.520
27	5579	0.483
28	6135	0.445
29	6725	0.408
30	7356	0.371
31	8000	0.335
32	8659	0.301
33	9333	0.269
34	10026	0.238
35	10745	0.209
36	11488	0.181
37	12270	0.154
38	13095	0.129
39	13976	0.105
40	14931	0.082
41	15987	0.060
42	17192	0.039
43	18633	0.019
44	20427	0.000

Vertical resolution is important to resolve boundary layers (particularly shallow marine layers), free tropospheric transport with minimal numerical diffusion, and stratosphere-troposphere exchange (STE) of ozone. Mathur et al. (2017) evaluated hemispheric model runs using both 35 and 44 vertical layers (Figure 2-1, Table 2-1) up to a model top at 50 mb (~20 km). They found much improved performance using 44 layers, particularly around the tropopause, and recommend the use of as many layers as practical to resolve the free troposphere and lower stratosphere. The 44 layers resolve the mid-troposphere with layer depths typically ~500 m ($\Delta x/\Delta z \approx 200$) like the configuration of Eastham and Jacob (2017). However, this $\Delta x/\Delta z$ ratio is less than the optimal range of 700-1500 later reported by Zhuang et al. (2017), which better preserve intercontinental plume coherence up to a week or

more. Based on the findings of Zhuang et al., vertical layers should be at most ~150 m thick in the mid-troposphere for horizontal resolution of ~1°. We adopted the 44 layer structure for H-CAMx as this is the maximum number of layers available in the EPA's 2016 hemispheric WRF dataset (Table 2-1). The issue of vertical resolution should be further investigated in future applications of H-CAMx.

2.2 Meteorology

EPA's 2016 hemispheric WRF outputs were processed through the WRFCAMx interface program. As described above, we matched every WRF layer to CAMx (no layer collapsing) to maximize meteorological consistency and minimize vertical diffusion of international transport plumes. We configured WRFCAMx to output optional diagnostic fields for QA/QC purposes and to provide needed inputs for natural emission pre-processors (as described below). These additional variables are not used by CAMx directly and include:

- 10-m U/V wind components (used for OCEANIC and WBDUST processors)
- 2-m temperature
- Surface downward solar flux
- WRF boundary layer depths
- CAMx boundary layer depths (according to Kv calculation method)
- Surface precipitation rate
- Vertically integrated total cloud optical depth
- Soil moisture (used for WBDUST processor)
- Convective cloud tops (used for LNOx processor)
- Convective available potential energy or CAPE (used for LNOx processor)

WRFCAMx was set to generate vertical diffusivity (Kv) fields by 2 different approaches, the CMAQ[1] method and the WRF YSU[2] method, to allow CAMx sensitivity testing for this important parameter. The Kv option based on turbulent kinetic energy (TKE) could not be used because WRF was not run with a TKE-based boundary layer parameterization. Surface snow cover processing with WRFCAMx included tracking cell-specific snow age each simulation day to support snow albedo calculations within CAMx that depend on both snow depth and age since last snowfall. The distributed version of WRFCAMx does not process sea ice cover over polar oceans. We therefore modified WRFCAMx to use WRF's time- and space-varying sea ice field to replace fractions of ocean cover in the daily CAMx landuse input files.

Deep convection is an important process at global scales as it provides an efficient mechanism to loft emissions and secondary pollutants for long-range transport in the upper troposphere. It is also an important process for returning globally-transported pollutant back to surface, and for chemistry and wet removal. At spatial resolutions of ~100 km, sub-grid convection likely comprises a large fraction of total convective transport. The CAMx Cloud-in-Grid (CiG) addresses sub-grid convective transport but WRF was not run with the specific cumulus parameterization that can drive the CiG. Therefore, we set WRFCAMx to diagnose sub-grid convective cloud data, and then subsequently applied the "cloud patch" within the KVPATCH vertical diffusivity adjustment program to increase vertical mixing through the depth of the diagnosed sub-grid convective clouds. The distributed version of the KVPATCH program only applies the "cloud patch" for over-land convection. Given the expanse of deep convective activity over the world's oceans, KVPATCH was modified to extend the "cloud patch" over water bodies.

[1] EPA's original K-theory mixing rates developed for the Community Multi-scale Air Quality (CMAQ) model.

[2] Yonsei University (YSU) boundary layer scheme.

All meteorological pre-processing activities were reviewed for quality assurance. This included independently checking program configurations and scripts, reviewing message files, and spot-checking resulting variable fields graphically for obvious problems or flaws. All program modifications were first tested functionally in ideal test bed configurations, and then operationally by inspecting results using actual hemispheric model data.

2.3 Emissions

2.3.1 Global Emissions

Ramboll prepared CAMx-ready emissions from EPA's 2016 hemispheric emission datasets. The specific inventory sources for these datasets are similar to those reported by Mathur et al. (2017), but with some modernization and enhancements. Generally, global anthropogenic emissions are based on the 2010 Emission Database for Global Atmospheric Research (EDGAR, 2019) Hemispheric Transport of Air Pollution (HTAP), version 2, which were projected to 2014 using and the Community Emissions Data System (CEDS; 2019). Specific regional inventories were incorporated for the US (2016 "fe" national platform), Canada (scaled from 2014), Mexico (scaled from 2008), and several inventories for Asia and China (2015). Natural emissions include wildfire emissions from a combination of the Fire Inventory from NCAR (FINN; NCAR, 2019a) and the EPA's 2016 US emissions inventory; biogenic emissions from the Model of Emissions of Gases and Aerosols from Nature (MEGAN v2.1; NCAR, 2019b) and the EPA's US Biogenic Emissions Inventory System (BEIS, EPA, 2019); and lightning NOx from monthly estimates reported by the Global Emissions Initiative (GEIA, 2019).

We converted these gridded and point source datasets from CMAQ CB6r3/AE6 speciation to CAMx CB6r4/CF speciation using the CMAQ2CAMx re-formatting tool.

2.3.2 Additional Natural Emissions

Important natural emission categories for hemispheric applications include biogenic sources, wildfires, lightning NOx, windblown dust, oceanic sources, and volcanoes. The EPA emissions database includes biogenic, wildfires and lightning NOx, which we have processed to CAMx-ready input files as described above. EPA did not include windblown dust or oceanic sources because those are estimated within their hemispheric CMAQ model. Also, EPA's emissions do not include volcanoes, which we also ignore in this project.

CAMx internally calculates emissions of oceanic inorganic iodine (Ix) because it depends on the rate of ozone deposition to ocean surfaces (other halogens are not considered in the CB6r4 chemistry mechanism used in H-CAMx). Other marine emissions including sea salt and dimethyl sulfide (DMS) were generated by our recently upgraded OCEANIC pre-processor, which reads meteorological data directly from CAMx input files to estimate those emissions. Sea salt emissions include wind-driven open-ocean emissions (Ovadnevaite et al., 2014) and surf zone emissions along coastlines (Gong, 2003; with 100% whitecap coverage). The recent addition of DMS emissions supports new DMS reactions in CB6r4 that form SO_2 and aerosol sulfate; the emissions algorithm uses monthly climatological oceanic DMS concentration data and emission parameterizations from Lana et al. (2011), McGillis et al. (2000), Kondo (1975), Liss and Merlivat (1986), Nightingale et al. (2000), and Saltzman et al. (1993).

We generated windblown dust emissions using our new WBDUST pre-processor, which reads meteorological data directly from CAMx input files to generate emissions of fine and coarse primary PM. The approach is based on the global EMAC (ECHAM/MESSy) chemistry-climate model (Klingmueller et al., 2017; Astitha et al., 2012).

All emissions pre-processing activities were reviewed for quality assurance. This included independently checking program configurations and scripts, reviewing message files, and spot-checking resulting variable fields graphically for obvious problems or flaws.

2.4 Initial/Boundary Concentrations

EPA applies "clean" lateral BC profiles along the equatorial boundaries, arguing that impacts from lateral BCs are generally confined to lower latitudes with little propagation into the domain. They also apply the same clean profiles for ICs, requiring a 12-month "spin-up" period prior to the actual simulation year of interest to reach a chemically mature characterization of the global atmosphere.

For this project, we decided not to use EPA's simple IC/BC fields, opting to generate them from pre-existing global model output. This approach (1) removes the arbitrary characterization of near-equatorial profiles, (2) provides a needed characterization of stratospheric ozone (as described below), and (3) dramatically shortens spin-up times since the initial state of the global atmosphere is already well-evolved. EPA has run the GEOS-Chem global model for 2016 to compare with their hemispheric CMAQ simulations. However, EPA only retained 3-hourly output for a sub-domain centered on North America. Therefore, we developed CAMx initial, lateral and top BCs from our own 2016 GEOS-Chem application that was recently completed for another project (Nopmongcol et al., 2019). We used our latest GEOS2AQM interface processor, adapted from a Python tool developed by Barron Henderson at EPA, that reads the GEOS-Chem netCDF output file format. A modification was necessary to allow for interpolation of GEOS-Chem data across the international date line (180° longitude). For top BCs, we extracted concentrations from GEOS-Chem layer 39 (20.4 km, 52.0 mb; see Table 1).

IC/BC pre-processing activities were reviewed for quality assurance. This included independently checking program configurations and scripts, reviewing message files, and spot-checking resulting variable fields graphically for obvious problems or flaws. All program modifications were reviewed by carefully inspecting results.

2.5 Other CAMx-Specific Inputs

Ramboll developed monthly-average total ozone column maps for the hemispheric domain to support the calculation of monthly photolysis rate lookup tables. Normally, we would obtain ozone column data from on-line archives of satellite-based Ozone Monitoring Instrument (OMI) measurements: ftp://toms.gsfc.nasa.gov/pub/omi/data/monthly_averages/ozone/. However, 2016 OMI data were missing for the month of July. We identified an alternative global ozone column database from a newer satellite sensor called the Suomi-NPP Ozone Mapping and Profiler Suite (OMPS): ftp://toms.gsfc.nasa.gov/pub/omps_tc/data/monthly_averages/ozone/. These data are provided in exactly the same format and global resolution as OMI. We used the CAMx pre-processor O3MAP to process OMPS data to CAMx input format.

We then ran the CAMx TUV pre-processor to generate monthly photolysis rates lookup tables for the CB6r4 chemistry mechanism. TUV uses the CAMx O3MAP files described above to define the range of monthly total ozone column for the photolysis rate calculations.

All pre-processing activities were reviewed for quality assurance. This included independently checking program configurations and scripts, reviewing message files, and spot-checking resulting variable fields graphically for obvious problems or flaws.

2.6 Modifying CAMx for Stratospheric Ozone

Stratospheric ozone presents several challenges for tropospheric photochemical modeling. First, stratospheric-tropospheric exchange (STE) is an important source of tropospheric ozone, but it is

complicated by the highly dynamic nature of the tropopause, which varies substantially with latitude and season together with short-term spatio-temporal undulations induced by mid-latitude baroclinic waves. These dynamics must be adequately resolved by the grid and properly addressed by the source of meteorological data that drives the chemical transport model. Second, models must chemically maintain or otherwise specify stratospheric ozone concentrations because stratospheric chemistry is distinctly different from tropospheric chemistry. Continental/regional-scale models can maintain stratospheric ozone concentrations without the need for chemistry because the residence time of stratospheric air is just a few days on these limited-area domains, and stratospheric ozone is continuously replenished via BCs.

To avoid complexities and extended run times from explicitly incorporating stratospheric chemistry, tropospheric chemistry models often implement diagnostic methods that specify stratospheric ozone concentrations or fluxes across the tropopause. One popular approach exploits observed correlations between lower stratospheric ozone concentrations and a conserved metric from fluid dynamics called "potential vorticity" (PV) that can be used as a tracer for stratospheric air. EPA has employed an approach for their hemispheric CMAQ applications that uses O_3:PV ratios to set ozone concentrations in stratospheric layers (Xing et al., 2016), where PV is determined by WRF. A similar approach could be adopted for H-CAMx, requiring modifications to both CAMx and the WRFCAMx interface program. While we recommend this for future H-CAMx applications we have not implemented a PV algorithm in this project.

Instead, we have leveraged an advantageous feature unique to CAMx: the ability to use time- and space-varying top BCs of stratospheric ozone. A new subroutine linearly interpolates ozone concentrations between the model top (via top BCs) and the layer just above the diagnosed tropopause in each grid column at each time step. The interpolation is conducted over height coordinates rather than pressure. The thermal tropopause is identified as the height at which the resolved vertical temperature gradient first exceeds -2K/km and extends above that level for at least another 2 km (WMO, 1992). Ozone concentrations in each layer above that point are reset to the linearly interpolated value. In this case, the top BCs are extracted from the same GEOS-Chem data used to derive initial and lateral BCs. Top concentrations are held constant between 3-hourly update times according to the frequency of global model output.

However, this method presents two disadvantages: (1) as with IC/BCs, H-CAMx must rely on output from another global model to supply top BCs, so H-CAMx is not an entirely independent model; (2) errors present in the external global model transfer to and propagate through the H-CAMx domain. Nevertheless, the second issue is not materially different from errors introduced by a O_3:PV scheme with its own inherent and explicit assumptions. Note also that any approach where ozone concentrations are simply diagnosed or reset (as described above) violates ozone mass conservation in stratospheric layers of the model. It is therefore useful to consider these approaches as a multi-layer dynamic BC input for the troposphere, where ozone mass is conserved.

To evaluate the efficacy of the linear interpolation approach, we tested CAMx using an existing 2014 regional modeling platform that we have recently developed for the Western Regional Air Partnership (WRAP). Limited-area regional modeling was selected for this test so that we could directly compare the unmodified case, where stratospheric ozone is constantly replenished solely from three-dimensional transport of lateral/top BCs, and the modified case, where stratospheric ozone is continually reset according to the method above. The closer the agreement between the two models, the more confidence we have that the simple treatment adequately characterizes lower stratospheric ozone in the uppermost layers of CAMx. In both cases, ozone top BCs were derived from a 2014

GEOS-Chem application, and CAMx was run over the 6-day period of April 15-20, 2014 on a North American 36-km modeling grid. Chemistry was turned off resulting in only transport.

Figure 2-2 presents test results against 2 North American ozonesonde profiles that were available during the simulation period. More importantly than whether the model adequately replicates the observed profiles, the test reveals that the modified and unmodified models do not differ substantially. Occasionally large variations between the two models do occur, depending on where the tropopause is diagnosed to exist according to the model layer structure (modified model) and how three-dimensional transport evolves the stratospheric ozone distribution (unmodified model). As shown in Figure 2-2, the top 3 CAMx layers above 9 km in this case span 3-4 km each, thus the simulated ozone profiles are smooth relative to the observed profiles plotted at 100-m resolution. As a result of the coarse layer structure, the higher stratospheric ozone in the unmodified case may be caused by numerical diffusion. The tropopause is diagnosed to exist in the topmost layer for much of the domain well south of the mid-latitude jet stream, thus no stratospheric adjustment is applied in that area and so the modified and unmodified models agree. In the northern portion of the domain, the tropopause can extend down to layer 21 (6-7 km) within deep troughs propagating across Canada and the upper Midwest US. In Figure 2-3, for example, the modified CAMx model increases stratospheric ozone just above the tropopause (layer 22) by 200-600 ppb (100-300%) within the Canadian trough. Surface ozone impacts remain nearly identical in both cases, differing by much less than 1 ppb. Overall, we saw no significant issues with employing this simple adjustment and conducted a more in-depth analysis with the H-CAMx (Section 3).

It was also necessary to modify the Ozone Source Apportionment Technology (OSAT) to accommodate the new stratospheric ozone module. The top boundary ozone tracer in every stratospheric layer of each grid column are reset to the new ozone values and all other ozone tracers are reset to zero. This approach conforms to the OSAT requirement that all tracers sum to the core-model value. Results of an H-CAMx SA demonstration are summarized in Section 4.

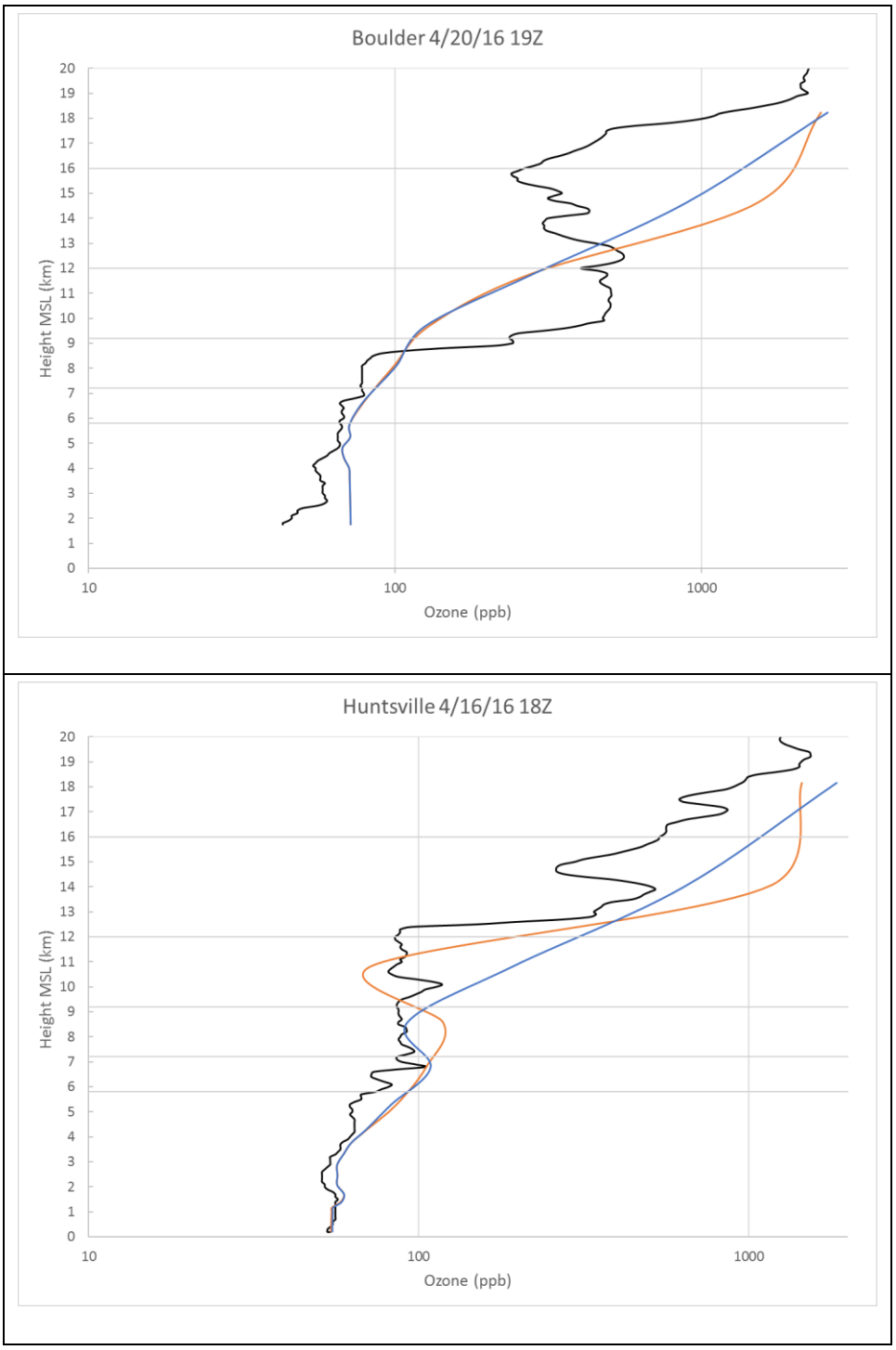

Figure 2-2. Ozone profiles at Boulder, CO (top) and Huntsville, AL (bottom): observed (black), unmodified CAMx (orange), and CAMx with linear stratospheric ozone between the model top and the diagnosed tropopause (blue). The top 5 CAMx layers (21-25) spanning 5.8-20 km are shown as horizontal grey lines to represent modeled resolution of the stratosphere.

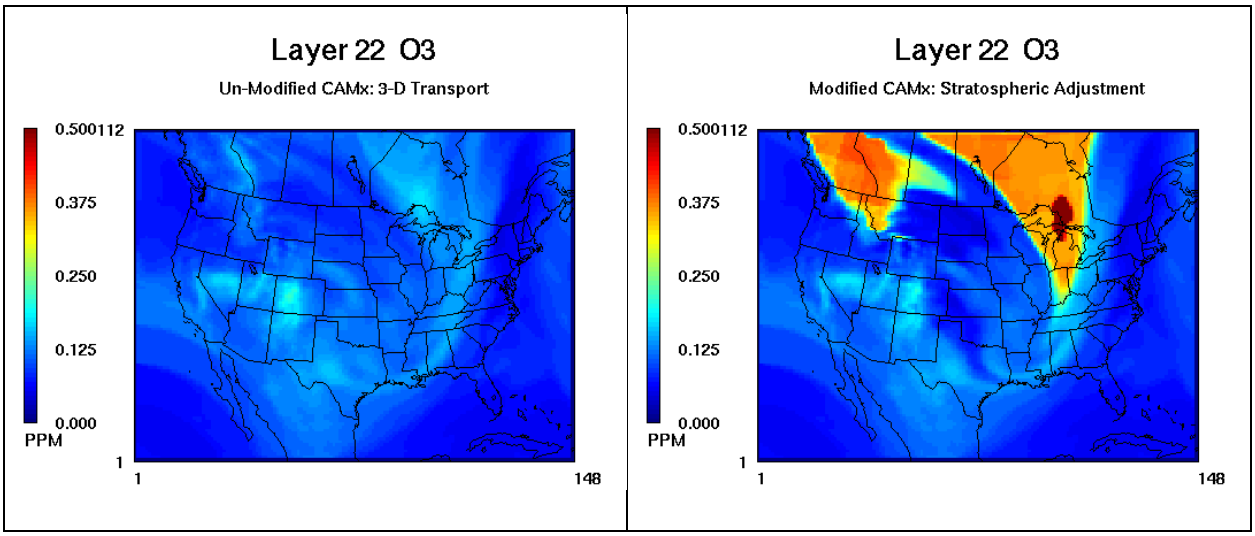

Figure 2-3. Comparison of upper-level ozone (layer 22; ~7-9 km) on April 15, 2014 at 18Z; unmodified CAMx (left) and modified CAMx (right).

3.0 H-CAMx APPLICATION AND EVALUATION

H-CAMx runs spanned May through September, 2016, with a one-month spin-up period (April) from ICs. Normally, global and hemispheric models must involve extensive spin-up times of up to a full year from a set of simple initial concentration distributions. Since we leveraged available global model output for 2016 that represents fully-evolved atmospheric chemistry, a much shorter hemispheric spin-up could be achieved. Additionally, at least one month was needed to ensure that international transport to Texas can be tracked up to May 1.

The two initial runs were inert so that we could quickly review the evolution of ozone initial, boundary and top concentrations and the influence of our stratospheric ozone treatment. One inert run included the stratospheric ozone treatment described in Section 2, while the other did not so that ozone in the stratosphere evolved strictly via dispersion of IC/BCs. Differences between the two were reviewed via graphical animations at the surface and at 4 upper layers (30, 35, 40, 44) ranging from the upper troposphere through the lower stratosphere to the top of the model. As described below, we evaluated both runs against ozonesonde data to assess which was more appropriately characterizing stratospheric and upper tropospheric ozone profiles. Based on that analysis, we chose to continue using the stratospheric ozone treatment. The final of the three runs was a full chemistry application of H-CAMx using the stratospheric ozone treatment. Performance results for that run against ozonesonde data are also described in the next section.

All H-CAMx simulations ran 183 days from April 1 through September 30 on two Intel Xeon E5-2690 2.60 GHz CPUs (24 virtual cores) with 132 Gb of total memory. CAMx was compiled using Portland Group Fortran90 v13.4 with OpenMP (OMP) shared-memory and Message Passing Interface (MPICH3) distributed-memory parallelization enabled. The full chemistry H-CAMx run used 8 MPI slices with 3 OMP threads each (24 cores total). The total full chemistry runtime for 183 simulation days was 2.7 days, with an average single-day runtime of 22 minutes.

3.1 Model Evaluation

The model performance evaluation was guided by EPA's Global-Scale Simulation Model Operational Evaluation Protocol (EPA, 2018), which was included in Appendix A of the Modeling Protocol. Ramboll considered the evaluation approach in consultation with the TCEQ project manager. We obtained 2016 global observational datasets from a parallel TCEQ project (WO 582-19-92775-04; Ramboll, 2019), which is supporting TCEQ's GEOS-Chem global modeling program. The model evaluation conducted under this project compared simulated ozone patterns against global ozonesonde measurements. We did not include a comparison to GEOS-Chem or EPA's 2016 hemispheric CMAQ results, as described in the Modeling Protocol.

Figure 3-1 compares domain-wide ozone patterns at three vertical levels (surface, layer 35 and layer 40) from the two inert H-CAMx runs. To reiterate, these inert CAMx runs only modeled the dispersion and surface deposition of ozone initial, lateral and top BCs over the April-September 2016 simulation period; there was no chemical production or removal of ozone. Layer 35 is ~10 km above sea level and is close to the mid- and high-latitude seasonal average tropopause altitude. Layer 40 is ~15 km above sea level, well into the lower stratosphere at most latitudes except perhaps near the equator. We chose to present a day in September to show the long-term evolution of differences between the stratospheric and no-stratospheric treatment. September 20 is shown specifically because the highest simulated surface ozone concentration occurred on that day (over the Himalaya Mountains). Figure 3-2 compares May-September averaged ozonesonde measurements to simulated ozone profiles from both inert runs at six selected global monitoring sites around the northern hemisphere. Figure 3-3

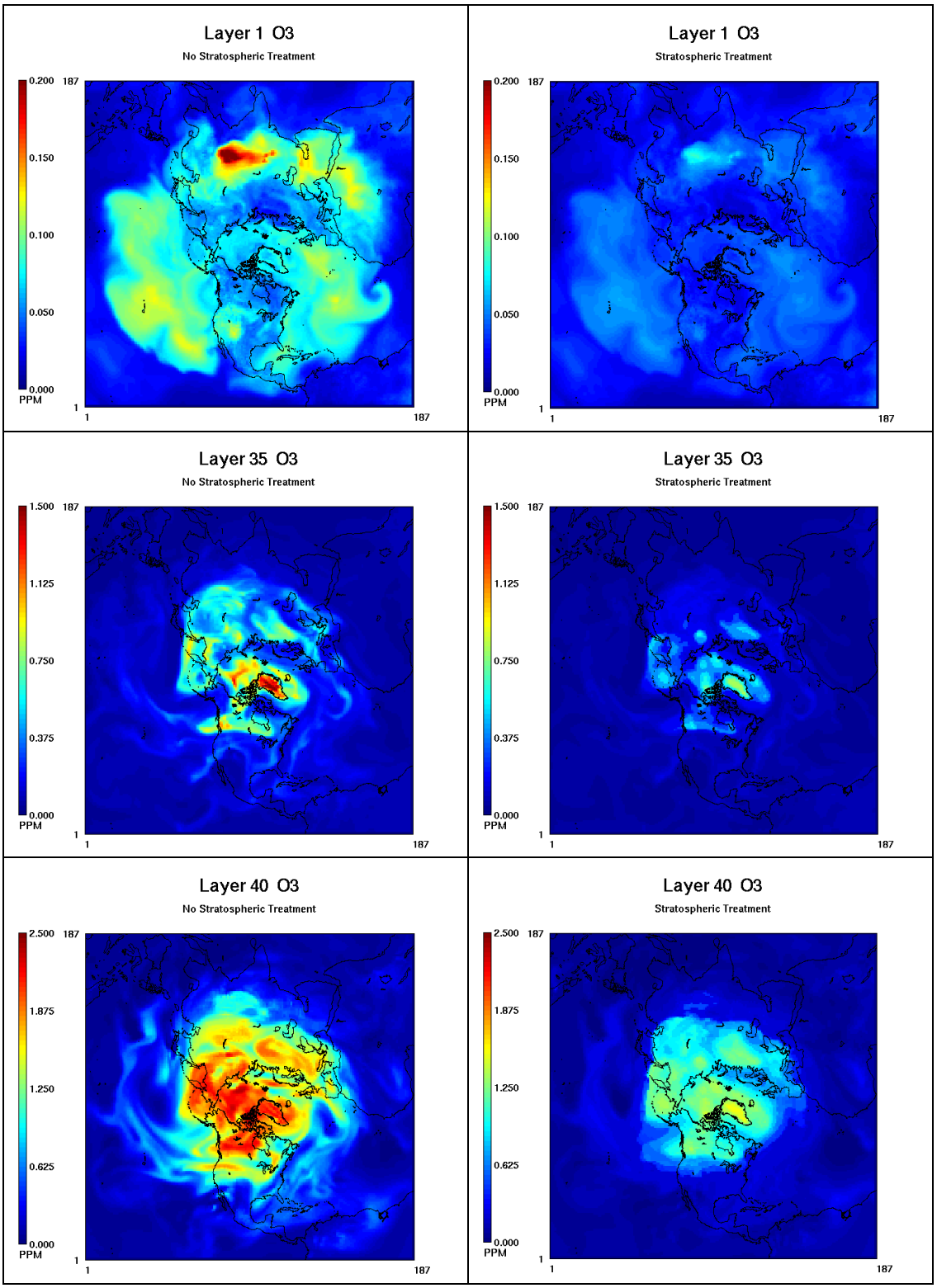

Figure 3-1. Ozone concentrations (ppm) over the H-CAMx modeling domain on September 20, 2016. Results are shown for the inert simulations, no stratospheric treatment (left) and with stratospheric treatment (right). Surface layer is shown in top row, layer 35 (~10 km) is shown in the middle row, and layer 40 (~15 km) is shown in the bottom row. Note different color scales for each layer.

shows the locations of each of the ozonesonde sites.

The most obvious and surprising feature in Figures 3-1 and 3-2 is the much higher ozone at most levels in the no-stratospheric treatment case. We had expected the stratospheric treatment would be needed to maintain high levels of ozone in stratospheric layers, while the no-treatment case would eventually lose its stratospheric ozone by intrusion into the troposphere with insufficient resupply from top BCs. In fact, the opposite occurs; in the no-treatment case, large influxes of ozone from the top boundary are transported into the upper layers and diffusively transported (both explicitly and numerically) into the troposphere. Note the rather unrealistically high and spatially expansive surface ozone concentrations greater than 100 ppb over the oceans in the no-treatment case, which are twice the magnitudes in the stratospheric treatment case. Once entrained into the shallow, stable marine boundary layers, these high ozone concentrations persist and build up for months given relatively slow depositional loss rates. Some of the downward diffusional transport may be caused by increased explicit diffusion in the cloud patching algorithm applied within deep convection. We did not conduct a test with cloud patching removed.

Conversely, the stratospheric treatment replaces the large top boundary ozone influx with a linear interpolation of concentration between the top BC and the tropopause, throttling the rate of tropospheric intrusion. Therefore, the treatment is not so much "maintaining" a stratospheric level of ozone but rather controlling the excessive entrainment of top boundary ozone. Yet the stratospheric treatment case continues to exhibit over prediction biases over May-September 2016, particularly in the upper troposphere and lower stratosphere, and even to the surface in oceanic areas such as shown at Hilo (Figure 3-2). Given the clearly better results using the stratospheric ozone treatment, we chose to continue to use it for the full chemistry simulation described below, and for the SA demonstration in Task 5. The remaining over prediction can be improved by applying an alternative altitude weighting in the stratospheric interpolation that leads to a "concave" profile shape that is typically seen in the ozonesonde measurements rather than the "convex" profile shape that results from diffusive vertical transport in CAMx.

Figure 3-4 compares domain-wide ozone patterns on September 20 at the same three vertical levels (surface, layer 35 and layer 40) from the inert and full chemistry H-CAMx runs, both using the stratospheric treatment. Figure 3-5 compares May-September averaged ozonesonde measurements to simulated ozone profiles from both runs. At the surface, the full chemistry run indicates much higher ozone than the inert run in eastern China, the Himalayas, the middle east, and northeast Africa. However, surface ozone is lower in the full chemistry run as a result of the extremely low NOx environment where photochemistry destroys ozone along with enhanced destruction by oceanic iodine emissions. In layer 35, ozone patterns are very similar between the inert and full chemistry runs, except for somewhat higher ozone by roughly 10-40 ppb over the mid-latitudes, presumably due to chemical production from anthropogenic precursor emissions. In layer 40, results from inert and full chemistry runs are practically identical as we would expect given that it is most often within the stratosphere.

Comparisons of inert and full chemistry CAMx results to ozonesondes in Figure 3-5 reinforce the differences described above. While simulated average ozone profiles are identical in the stratosphere above 100 mb (~16 km), ozone tends to be higher in the full chemistry run throughout the troposphere at most sites by several tens of ppb. This results in a modest increase in the general over predictions seen in the inert results. The only exceptions to higher tropospheric ozone occur at Lerwick, the northernmost site, where the average ozone profile is little different from the inert run, and in the marine boundary layer at Hilo due to the oceanic chemical environment.

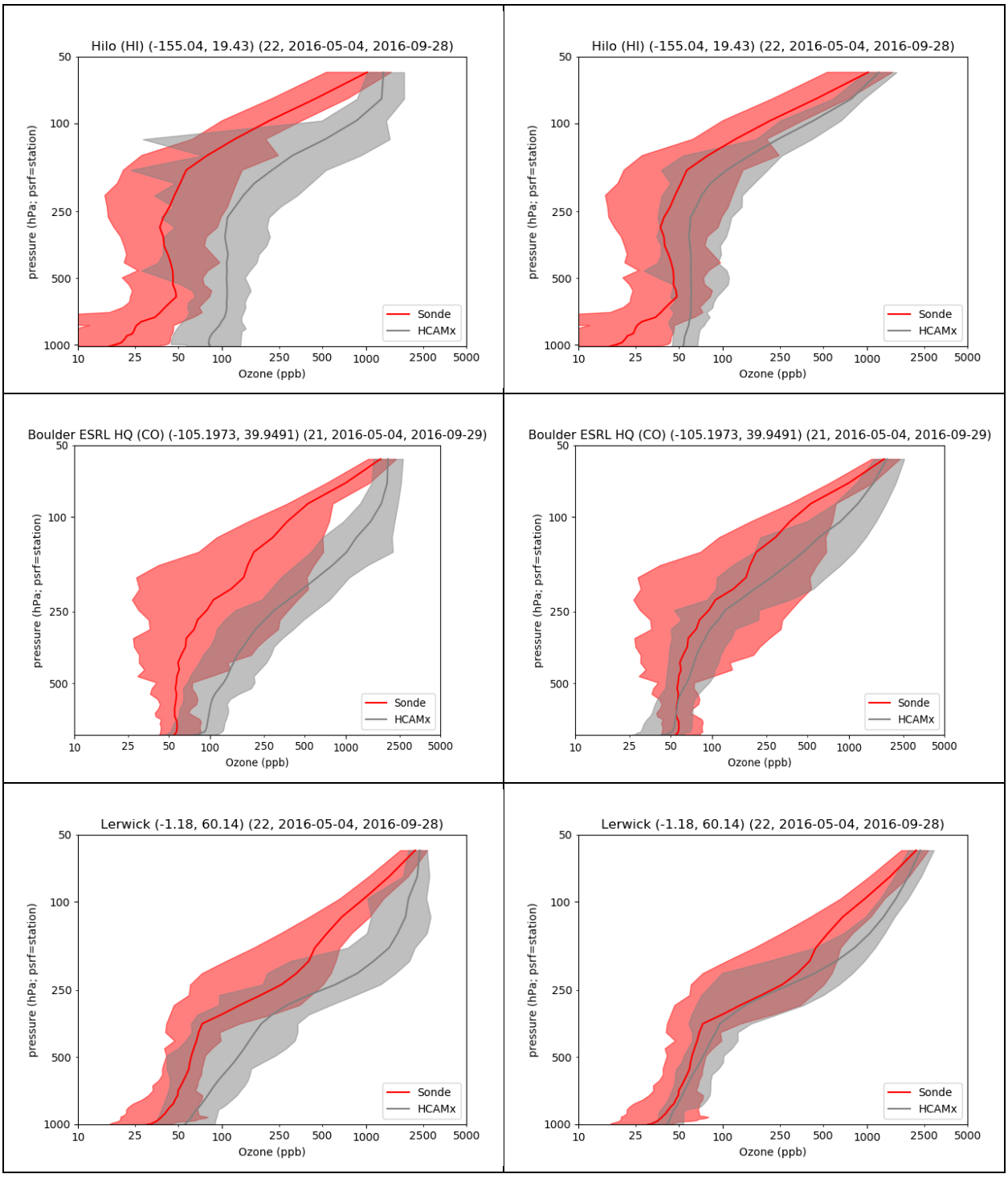

Figure 3-2. Comparison of selected ozonesonde profiles (red) and CAMx inert runs (grey) using no stratospheric treatment (left) and using a stratospheric treatment (right). Solid lines show the average, shading shows the minimum to maximum range. The order of plots from top to bottom move from west (Hilo, HI) to east (Sapporo, Japan). These sites were selected based on data availability in 2016 and for dispersed spatial sampling of the northern hemisphere. Number of ozonesondes with date ranges are shown at the top of each plot, along with the station's longitude and latitude.

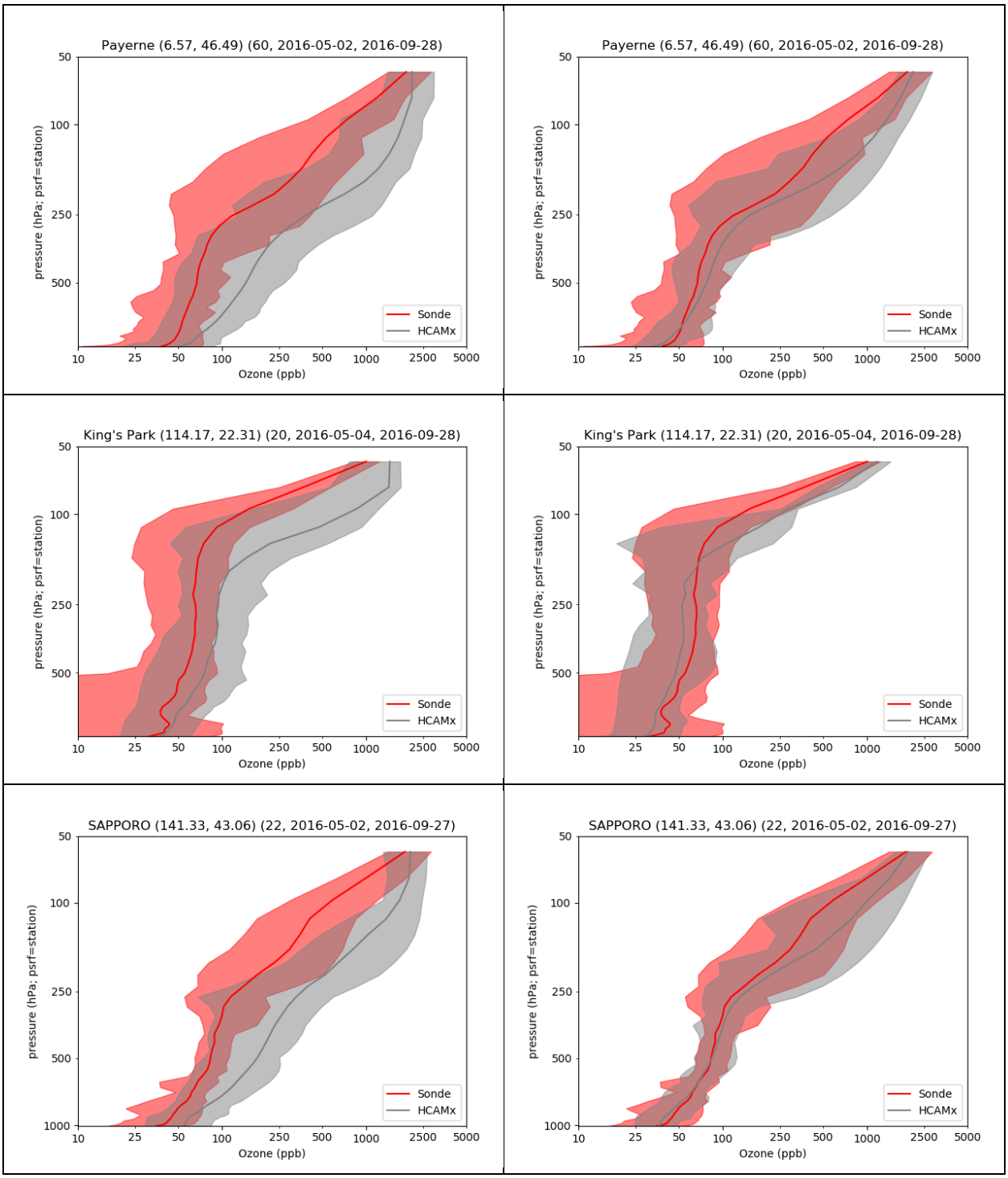

Figure 3-2 (concluded).

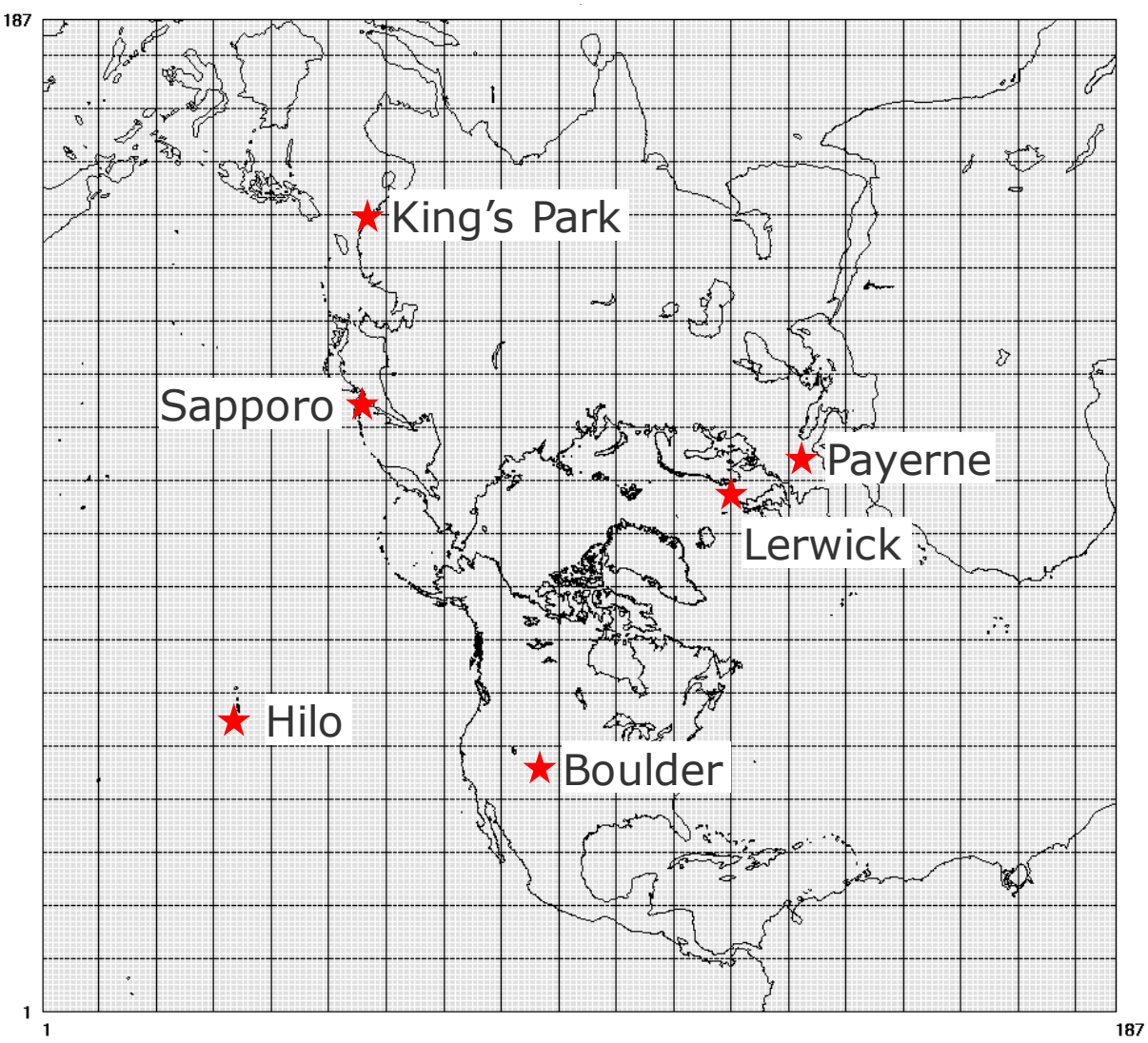

Figure 3-3. Location of ozonesonde sites shown in Figure 3-2.

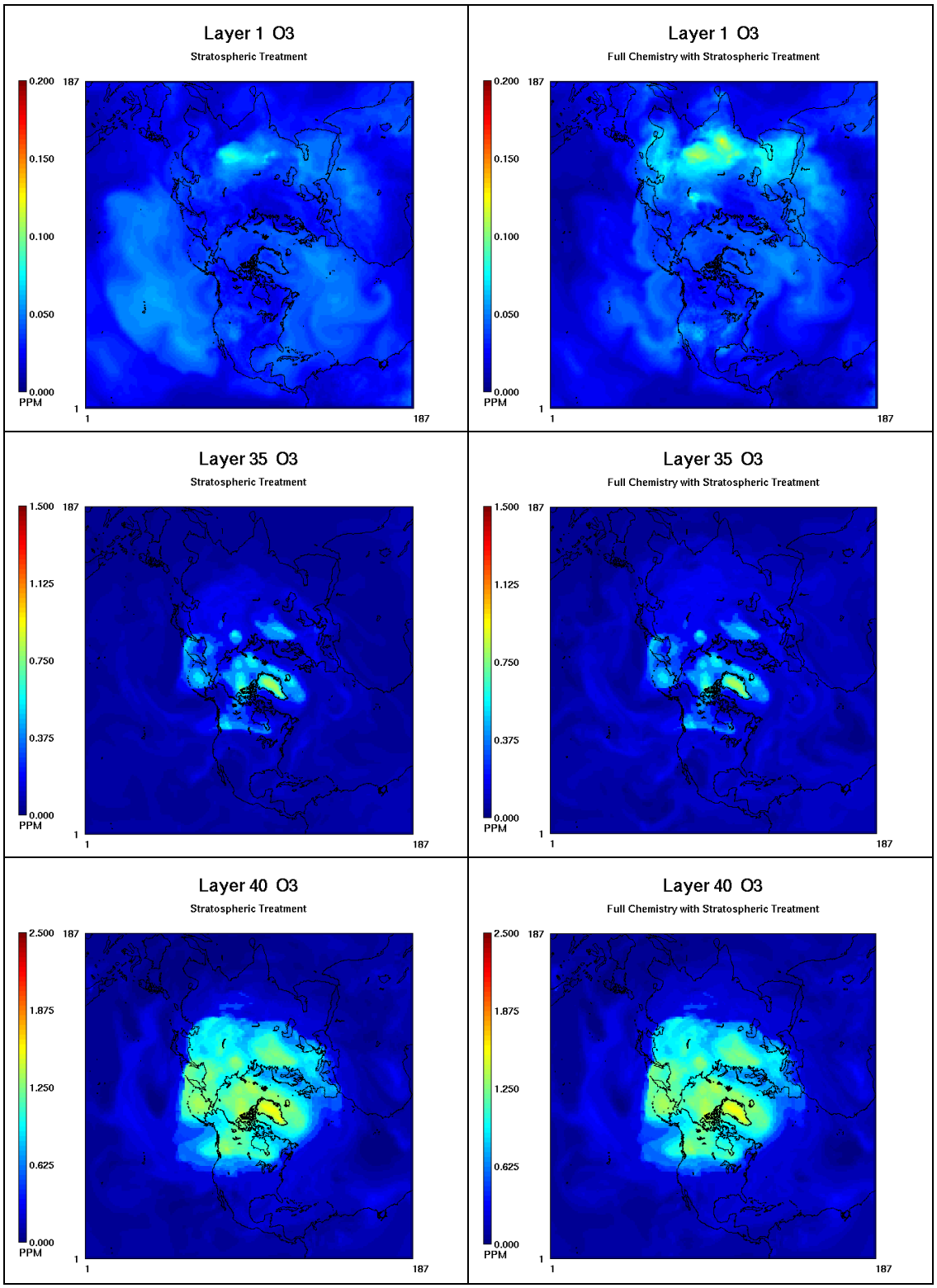

Figure 3-4. Ozone concentrations (ppm) over the H-CAMx modeling domain on September 20, 2016. Results are shown for the inert simulation (left; same as in Figure 3-1) and the full chemistry simulation (right), both with stratospheric treatment. Surface layer is shown in top row, layer 35 (~10 km) is shown in the middle row, and layer 40 (~15 km) is shown in the bottom row. Note different color scales for each layer.

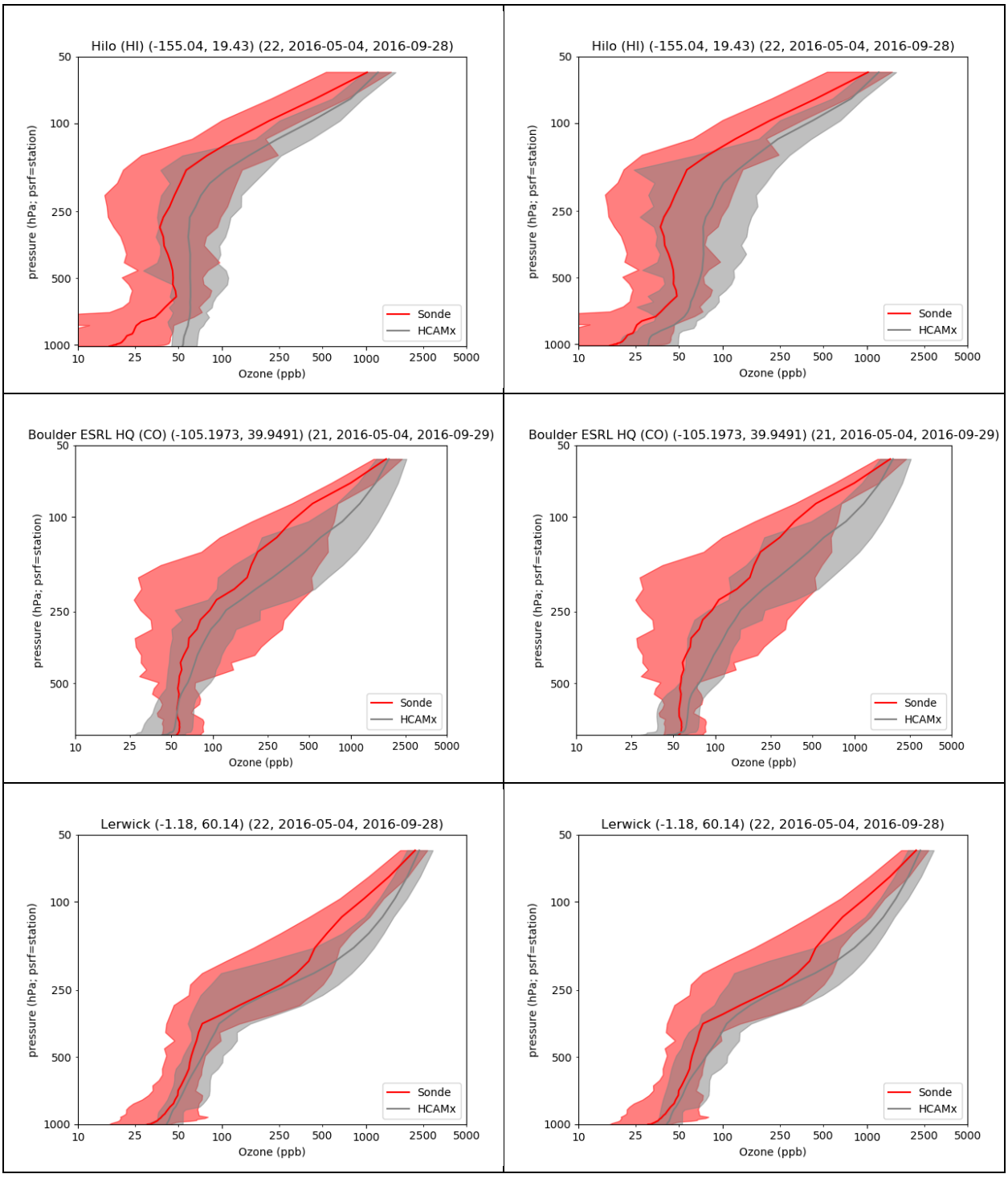

Figure 3-5. Comparison of selected ozonesonde profiles (red) and CAMx runs (grey) for the inert case (left; same as Figure 3-2) and the full chemistry case (right), both using a stratospheric treatment. Solid lines show the average, shading shows the minimum to maximum range.

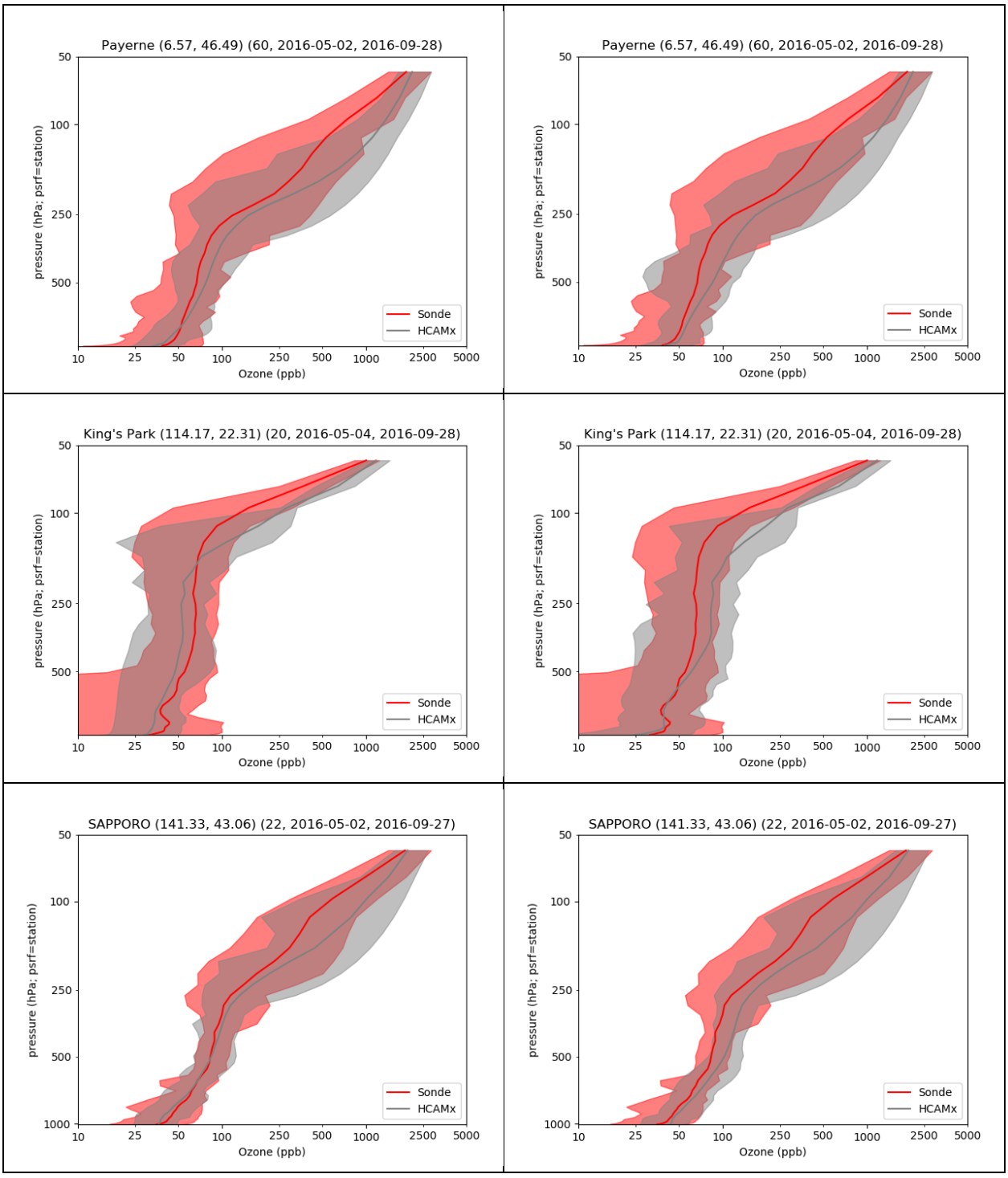

Figure 3-5 (concluded).

Given the tendency for slightly larger ozone over predictions throughout the troposphere and around the world in the full chemistry run, the role of the stratospheric ozone treatment takes on greater significance than we had anticipated. We implemented and tested an alternative ozone interpolation approach in the stratospheric treatment, one that replaces linear distances with cubed distances, which results in weighting ozone concentrations more toward the value at the tropopause. A similar effect could be achieved by linearly interpolating over pressure since it varies logarithmically with height, but that would result in a weaker "bend" in the ozone profile than using cubed altitude.

Figure 3-6 shows the resulting ozonesonde comparisons using the alternative stratospheric treatment in the full chemistry H-CAMx simulation. As expected, mean tropospheric ozone profiles and seasonal ranges are in much better agreement with observations at all sites. However, stratospheric ozone is consistently under predicted and this may have negative ramifications for properly characterizing contributions from resolved stratospheric intrusions, as opposed to reducing numerical diffusion of stratospheric ozone into the troposphere. Perhaps employing a squared rather than cubed distance interpolation would alleviate the under predicted stratospheric ozone profile, but at the expense of somewhat higher tropospheric ozone. Since it is more important to properly simulate the range of tropospheric ozone in H-CAMx for the purposes of supporting TCEQ regional modeling, the CAMx model code delivered to TCEQ for this project includes the cubic interpolation rather than the linear interpolation.

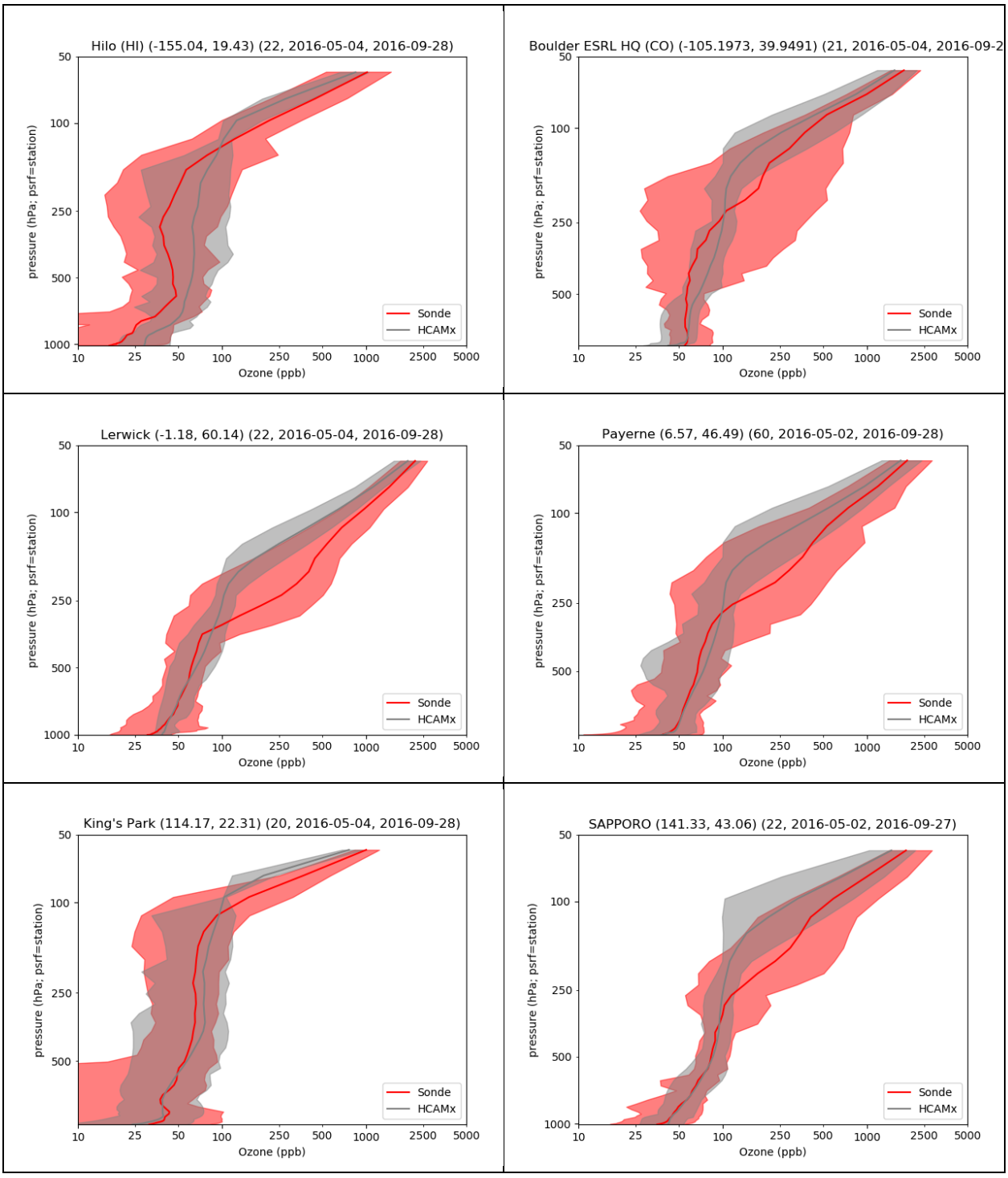

Figure 3-6. Comparison of selected ozonesonde profiles (red) and CAMx runs (grey) for the full chemistry case using the alternative stratospheric treatment. Solid lines show the average, shading shows the minimum to maximum range.

4.0 OZONE SOURCE APPORTIONMENT

This project included the use of source apportionment to quantify foreign contributions to ozone concentrations in Texas ozone nonattainment areas. As part of this work, we expanded the CAMx SA tool to allow for 1-way nesting of SA tracers via IC/BC. For example, a CAMx SA model application for the continental US can now read source apportioned BC files and track ozone and PM contributions from areas outside the continental US. The source apportioned BC files can be prepared from global model zero-out runs or an H-CAMx SA simulation. Ramboll has conducted functional testing of the model updates. We have delivered new CAMx and IC/BC interface pre-processor code to TCEQ for additional testing and use.

4.1 H-CAMx Source Apportionment Application

We used CAMx OSAT to track ozone contributions from six regions of the northern hemisphere (Figure 4-1) as well as the initial and boundary concentrations. OSAT tracked only a single emission sector (all anthropogenic and natural emissions combined) for efficiency and because we are interested in geographic contributions to ozone. For each of the six regions, plus IC and BC (8 tags in total), OSAT tracked NOx (N tracer), VOC (V tracer), ozone from NOx-limited chemistry (O3N tracer), ozone from VOC-limited chemistry (O3V tracer) and several grouped NOy compounds to account for "NOx-recycling" during long-range transport of aged emissions. OSAT could be used in H-CAMx to resolve ozone contributions from separate source categories, for example to separate ozone contributions of anthropogenic from natural sources using the APCA option. The "stratify-by-boundary" option could be used to separate ozone influx from the top boundary (i.e., the stratosphere) from the lateral boundaries. The coarse grid resolution of H-CAMx provides limited resolution of international borders, e.g., the US/Mexico border as illustrated by Figure 4-2, which would be alleviated by nesting the TCEQ's regional CAMx model within H-CAMx.

We ran H-CAMx/OSAT for the month of September 2016 including a 10-day OSAT spin up period from August 16. We selected September because it was the only month in 2016 when ozone levels in Texas were moderately elevated. This OSAT demonstration employed the initial stratospheric treatment because it was run prior to developing and testing the revised stratospheric treatment. We set ICs on August 16 from the H-CAMx full chemistry instantaneous restart file on August 15. The OSAT simulation ran on the same machine with the identical parallelization configuration as the full chemistry runs described in Section 3. The total OSAT runtime for 46 simulation days was 1.1 days, with an average single-day runtime of 35 minutes.

Figures 4-3 and 4-4 present surface ozone contributions from each of the 6 regions and IC/BCs, over the H-CAMx modeling domain on September 20, 2016, consistent with plots shown in Section 3. ICs persist from the model start on August 16 and are confined to mid and polar latitudes at concentrations below 15 ppb. BCs ranging up to 50 ppb cover the entire domain, where the highest concentrations occur along the domain boundaries (lateral BCs) and over the Himalayas (top BCs). Some moderately high contributions of ~30 ppb from the top BCs are also evident over the western US. The model shows that Asia and the US have the most wide-spread contributions of all individual emission regions of the hemisphere, while much smaller contributions are simulated from Latin America and Canada. Contributions from the rest of the hemisphere (ROH) are highest in Eurasia, middle east, Africa, the Mediterranean, the Caribbean and Gulf of Mexico, and Indonesia through the Philippines. Some moderately high (~20 ppb) contributions from the ROH are also evident across the Pacific and Atlantic Oceans.

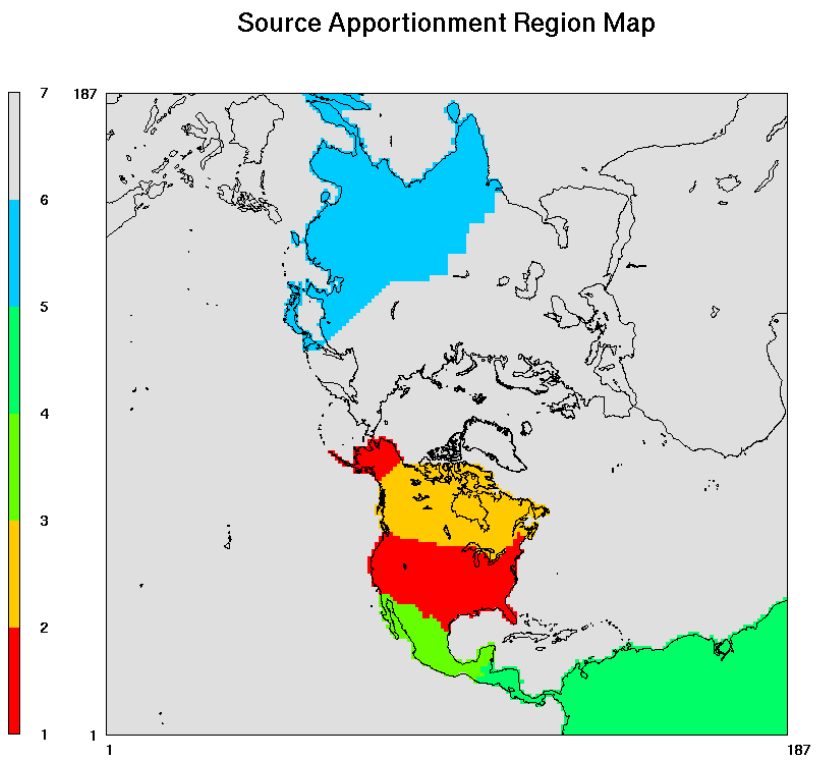

Figure 4-1. H-CAMx source apportionment emission regions: US, Canada, Mexico, Central and South America, southeast Asia and all others.

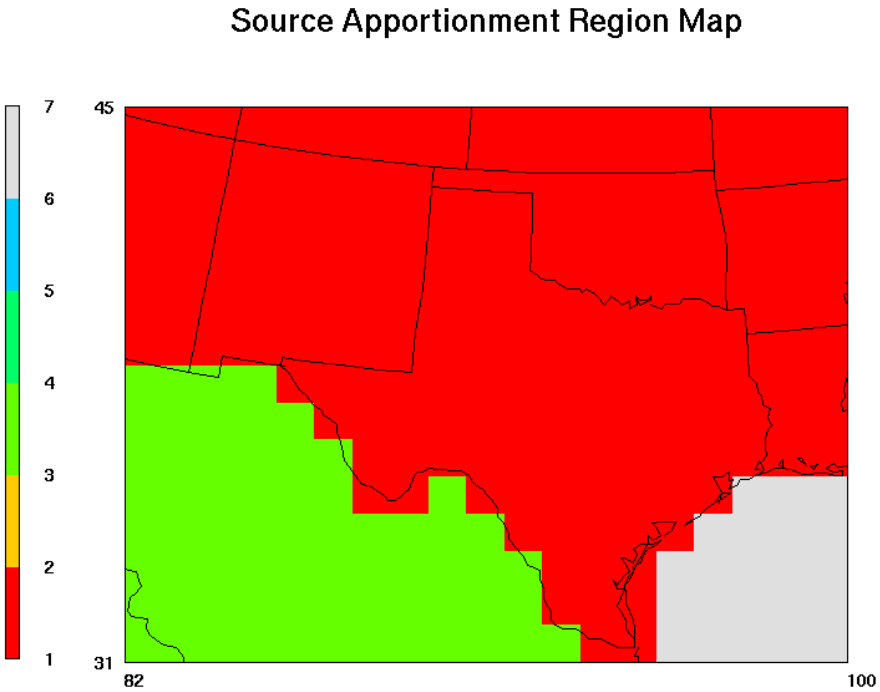

Figure 4-2. Enhanced view of H-CAMx source apportionment emission regions along the Texas-Mexico border, showing how the coarse hemispheric grid resolves the assignment of emissions between the two countries and Gulf waters.

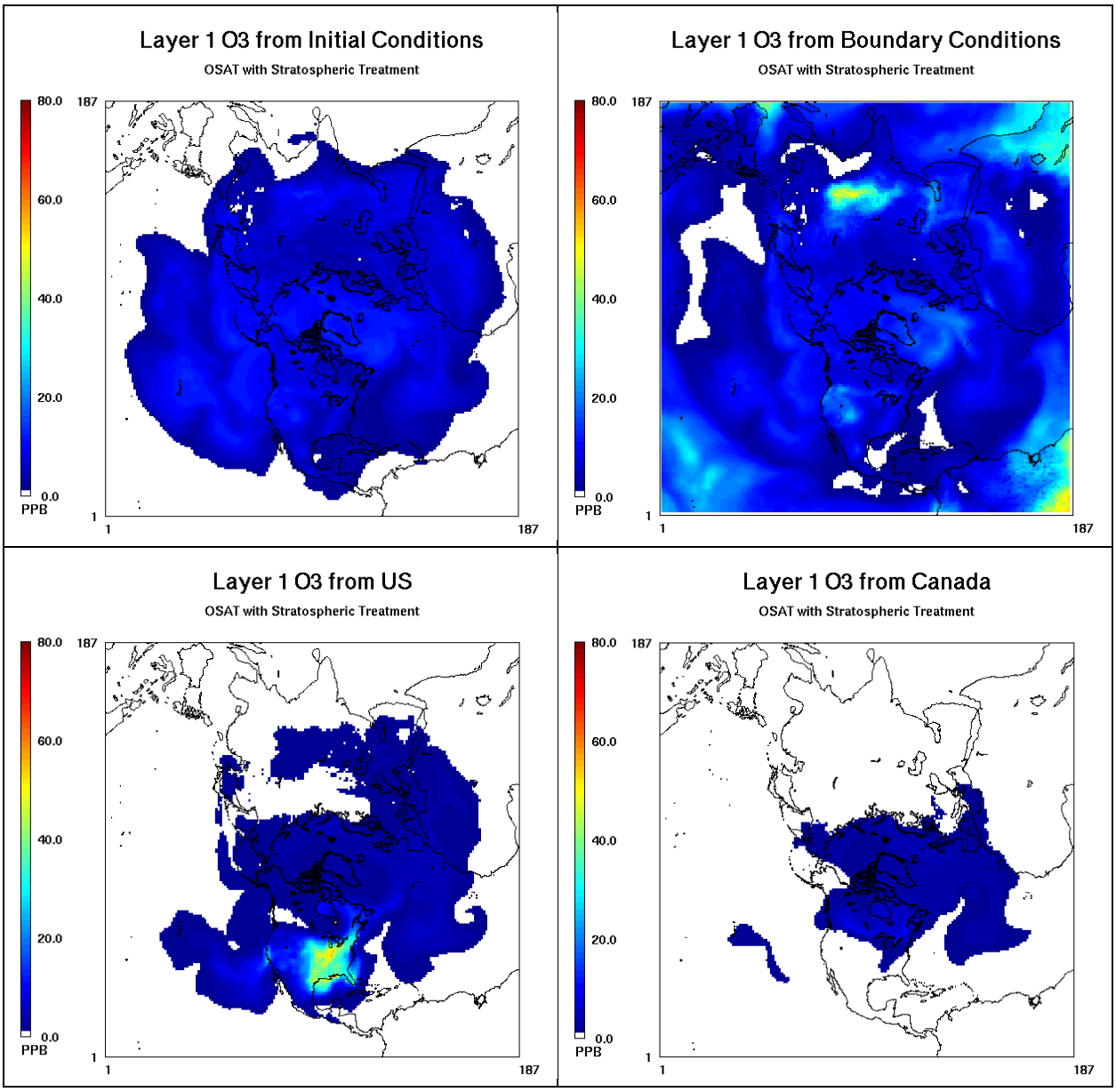

Figure 4-3. Surface ozone contributions (ppb) over the H-CAMx modeling domain on September 20, 2016: initial concentrations (top left), boundary concentrations (top right), US contributions (bottom left), Canada contributions (bottom right).

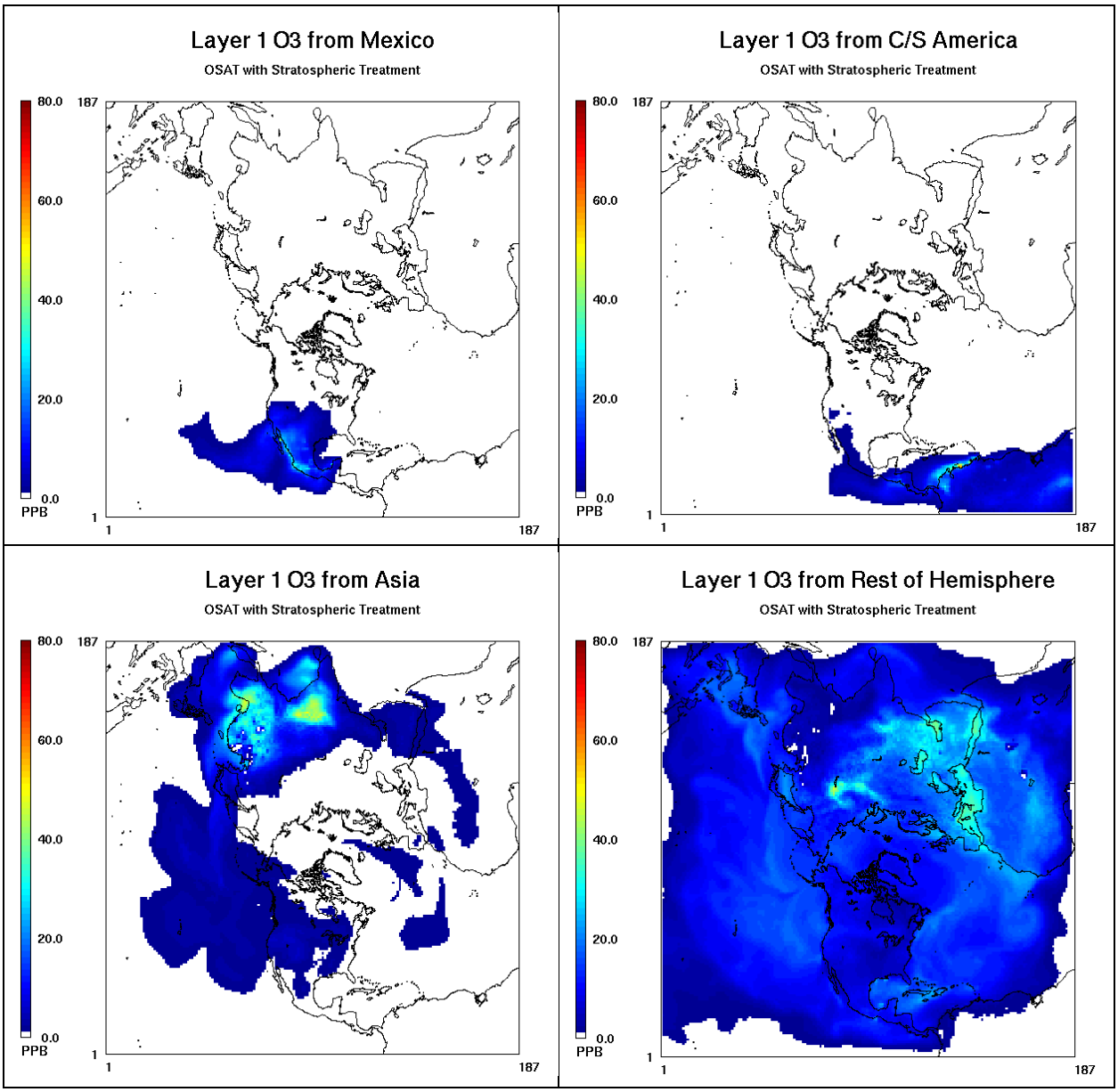

Figure 4-4. Surface ozone contributions (ppb) over the H-CAMx modeling domain on September 20, 2016: Mexico contributions (top left), Central and South America contributions (top right), Asia contributions (bottom left), rest of hemisphere contributions (bottom right).

Figure 4-5 shows time series of contributions to maximum daily 8-hour (MDA8) ozone from the six regions and IC/BCs in four Texas ozone nonattainment areas: Houston, Dallas, San Antonio and El Paso. These time series are arranged as "landscape" plots, which shows both the individual and cumulative contributions to total simulated MDA8 ozone at each location. We extracted ozone values from the single grid cells containing each urban center. In all cities except for El Paso, US emissions are by far the dominant contributor, with large contributions from the ROH region (5-10 ppb) and IC/BCs, and occasional contributions from Mexico up to 5 ppb. In El Paso, a larger mix of contributors is evident, including the US reaching 25 ppb and Mexico reaching 15 ppb. Contributions from Canada, Asia and Latin America are negligible to small in all cases.

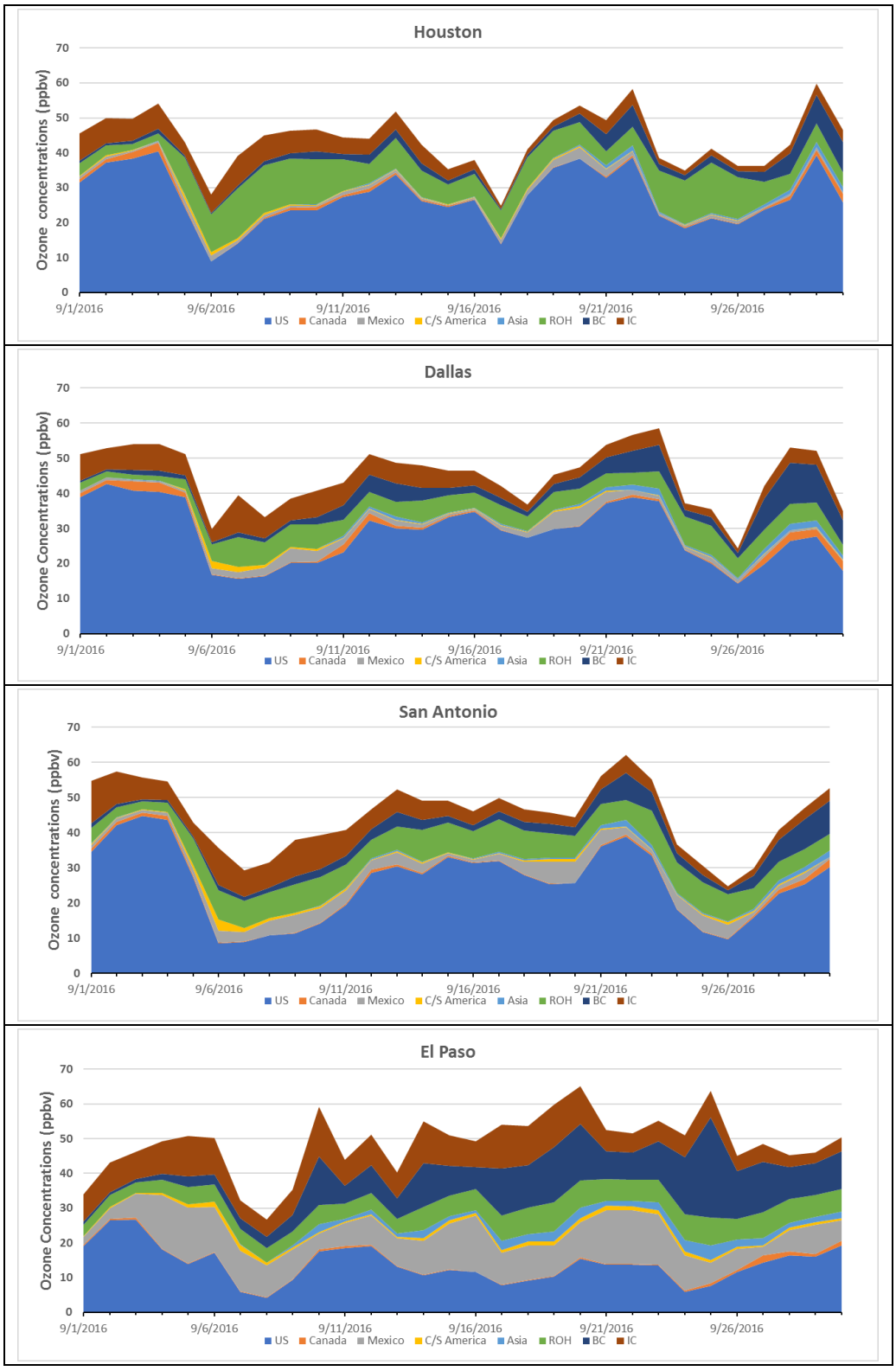

Figure 4-5. Time series of simulated ozone contributions from six regions of the northern hemisphere, and initial/boundary concentrations, over the month of September 2016. Plots are arranged so that the contributions from each source adds toward the total ozone simulated at each location, which is shown as the value at the top of the "IC" category.

Overall, results from the H-CAMx OSAT demonstration indicate that the model works as intended and will provide useful information about foreign contributions to Texas ozone in more detail, and more efficiently, than is possible using global models and brute-force (zero-out) emission perturbations. Initial concentrations of ozone persisted in the demonstration run but would dissipate in longer production runs. Ozone top boundary (i.e., stratospheric) contributions were larger near high terrain, which is an expected result, although we recommend more evaluation of the stratospheric contributions to ground-level ozone in H-CAMx. The contributions among the US, Mexico and Latin America could be refined by downscaling these course hemispheric OSAT results to a nested 36/12/4 km regional modeling application via 1-way BCs. Longer seasonal H-CAMx OSAT runs would better resolve the contributions from ICs into the six source regions and BCs. Stratifying BCs to the four lateral and single top tracers would provide additional information on the role of downward tropospheric intrusion of stratospheric ozone.

4.2 CAMx Updates to Support SA IC/BC

Traditionally, CAMx SA separately tracks contributions from ICs and BCs supplied to the core model for the master (outermost) domain. The IC/BC tracers yield no information about where their contributions originated (there is a "stratify by boundary" option for BC apportionment that we omit from this discussion because it offers limited information). Consequently, in the case of 1-way nested simulations, there is no mechanism for passing SA information from the coarser grid to the nested grid via the BCs. A CAMx update was needed to allow IC and BC files to transfer SA contributions from a larger/coarser domain to a smaller/finer 1-way nested domain. Additionally, this update needed to accommodate the ability to transfer contributions derived using global models (i.e., via emission "zero-out" runs) to CAMx SA IC/BC inputs for continental/regional CAMx SA applications.

Ramboll developed an approach to handle both cases: (a) CAMx SA 1-way nesting and (b) interfacing global model output to CAMx SA applications via BCs. The approach required new IC/BC interface programs, as well as extensive updates to CAMx to read new SA IC/BC inputs without major disruptions to the traditional manner in which SA has been used. Figure 4-6 presents a general flow diagram for the 1-way nested SA process. Note that the top portion of the diagram shows a CAMx-to-CAMx 1-way nesting process, while the bottom portion shows how SA IC/BC are developed from multiple global model simulations.

4.2.1 Interface Processor

The approach to interface H-CAMx output to regional applications via 1-way nested IC/BCs needs to address the following: (1) differing map projections/resolutions; (2) differing layer structures; (3) different time zones; and (4) SA tracers. Ramboll uses a program called BNDEXTR that supports separate, 1-way nested CAMx applications by converting three-dimensional output from a coarse grid run to IC/BCs for a fine grid run. It is designed to maximize flexibility among grid projections and horizontal resolutions: it interpolates three-dimensional concentration data from one projection/resolution to IC/BCs on a totally different projection/resolution as long as the target grid fits within the larger grid. It also generates time-varying BCs according to the coarse grid output frequency, so if H-CAMx outputs data at 3-hourly intervals, BCs would be derived at those frequencies. To maximize chemical consistency between global and regional simulations, the same chemistry mechanisms need to be employed in both cases because BNDEXTR transfers all species concentrations to IC/BC input files with no unit conversions or species mapping. The original BNDEXTR assumed identical layer structures and time zones between the two grids; in this project, Ramboll updated the BNDEXTR program to accommodate different layer structures and time zones for increased flexibility. Additionally, we updated BNDEXTR to process three-dimensional gridded SA

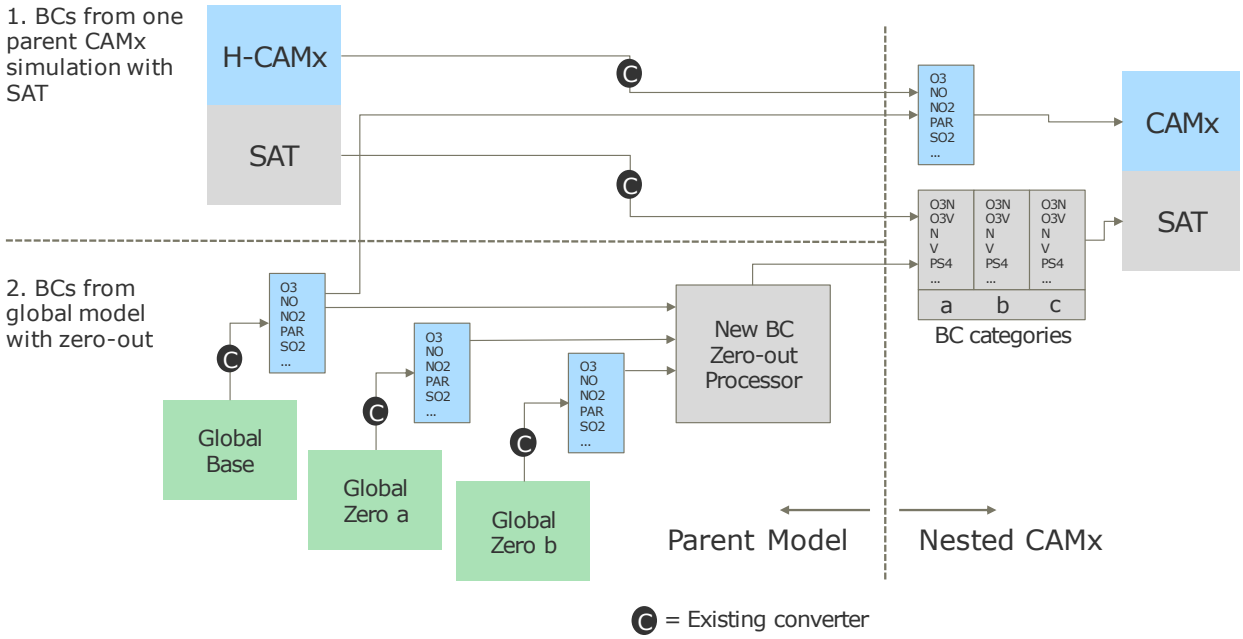

Figure 4-6. Schematic of data flow and processing for 1-way nested source apportionment boundary concentrations. The top section shows a 1-way CAMx-to-CAMx case (e.g., hemispheric to regional, or regional to urban); the bottom section shows a case in which a set of global model zero-out runs (e.g., from GEOS-Chem) are combined and transferred to a CAMx source apportionment run.

tracer output from an H-CAMx run to a new specialized set of SA IC/BC inputs for a 1-way nested regional run (as depicted in the top portion of Figure 4-6).

Note that the new BNDEXTR program expects to read CAMx standard and SA three-dimensional output concentration files in the netCDF format, either v3 or v4 (compressed or uncompressed) because that format contains vital grid and topographic information. However, BNDEXTR continues to write IC/BC files for both the standard model and for SA in the traditional CAMx Fortran binary format (also referred to as UAM format). The input files required for each run of BNDEXTR include:

- 3-D average output concentration file from a previous large-scale CAMx run containing standard model species or SA tracers (CAMx netCDF v3 or v4 format);
- 3-D meteorological file for the target nested grid (CAMx Fortran binary format) to define the map projection, 3-D domain/grid, time zone, and date/time span;
- 2-D surface/landcover file for target nested grid (CAMx Fortran binary format) to define the gridded topographic heights

Each run of BNDEXTR generates a BC file for the date/time span of the 3-D meteorological file, and optionally an IC file for a user-specified date/time, all of which are time-shifted from the CAMx 3-D concentration output files.

When reading a 3-D SA output file, BNDEXTR relabels each tracer from its original name, which contains species, emission category index and region index, to a new IC or BC name where each category/region pair is combined into a new single index. In this way, no category/region information

is lost, just renumbered to fit the requirements unique to IC/BC tracer names. For each SA group generated, a set of IC/BC tracer class names are generated with the following format:

SSSeeerr

where: **SSS** = tracer class
eee = SA group
rr = "IC" or "BC"

BNDEXTR echoes the mapping from 3-D SA tracer output names to IC/BC tracer input names as a record of this translation. As an example, say that CAMx SA is run tracking emissions from 3 source categories and 2 regions. The O3N tracer class (ozone formed from NOx) will be relabeled to 6 new names as shown below:

O3N001001 → O3N001IC (category 1, region 1)
O3N002001 → O3N002IC (category 2, region 1)
O3N003001 → O3N003IC (category 3, region 1)
O3N001002 → O3N004IC (category 1, region 2)
O3N002002 → O3N005IC (category 2, region 2)
O3N003002 → O3N006IC (category 3, region 2)

BNDEXTR generates SA IC/BC files that include only the tracer classes found in the 3-D files provided to it; therefore, if only OSAT is run then SA IC/BC tracers are generated only for the ozone and relevant precursor classes present, and no PM or its precursor tracers are generated for the 1-way CAMx nest. BNDEXTR echoes important diagnostic messages to the standard output on which species are found on the input files, and how they are mapped to the SA IC/BC tracer names. It also generates summary output of statistics for each species or tracer processed on each grid boundary for QA/QC review.

Ramboll tested and quality-assured the BNDEXTR preprocessor using output from the 2016 H-CAMx run described above. We have delivered the BNDEXTR program to TCEQ for their testing and use with the H-CAMx output.

4.2.2 CAMx Updates

Several major updates to CAMx were necessary to support the new 1-way nested SA IC/BC capability. First, we modified CAMx to optionally output 3-D, time-varying SA tracer concentrations (historically only 2-D surface fields were output) to allow for development of SA IC/BC inputs for downstream 1-way nested runs. Second, we modified CAMx to read the new SA IC/BC input files and include the tracer species names found in the IC/BC files in the list of tracer species for the nested CAMx SA simulation (in place of the traditional IC/BC tracer names). Note that IC/BC tracers supplied through IC/BC files are carried throughout the master and all 2-way nested CAMx grids just as in the traditional approach. The updated CAMx version optionally allows either the traditional approach for IC/BC apportionment or the new apportioned IC/BC tracers using input files from the SAICBC program.

Ramboll tested the updated CAMx version as part of a parallel project conducted for the EPA, using model inputs for their 36/12 km nested North American grid (2016 modeling platform). We have delivered the updated CAMx code to TCEQ for their testing and use, which includes the CAMx code updates described in earlier sections to support H-CAMx.

5.0 CONCLUSION AND RECOMMENDATIONS

This project successfully developed an application of H-CAMx for the May-September 2016 season, including an example OSAT run for the month of September 2016, using hemispheric emissions and meteorological inputs developed by the US EPA. We derived initial/boundary conditions from an existing 2016 GEOS-Chem global model run and developed oceanic and windblown dust emissions using Ramboll's latest emissions pre-processors. Additionally, the H-CAMx application required updates to the CAMx model and certain support programs. All updated model and processor codes have been delivered to TCEQ. All H-CAMx input/output files, source apportionment boundary conditions for the 36 km TCEQ regional modeling grid, and an updated User's Guide have also been delivered to the TCEQ.

With adjustments to the stratospheric ozone treatment, model results for ozone throughout the troposphere are reasonable and compare well with ozonesonde measurements from around the northern hemisphere. When parallelized over 24 CPU cores, H-CAMx run times are much faster (22 minutes/day) than GEOS-Chem runs using 2x2.5 degree horizontal resolution, 72 vertical layers, and its standard chemistry mechanism (~46 minutes/day using 48 cores on the same chipset as H-CAMx). The addition of our specific OSAT configuration increased run times by only 60% (35 minutes/day). Identifying and implementing additional speed enhancements (as listed below) would allow for improved grid resolution and larger SA applications while minimizing impact on model speed.

Based on results of this project, we recommend the following updates, analyses and applications:

- Develop and evaluate the use of satellite data products to derive lateral and top boundary concentrations and reduce H-CAMx reliance on other global models; ozone from NASA AIRS/OMI product (https://tes.jpl.nasa.gov/science/highlights/aura-highlights), carbon monoxide from MOPITT product (https://www2.acom.ucar.edu/mopitt), climatology for methane, and default small values for other compounds (e.g., NOy, VOCs and PM);
- Run alternative simulations of WRF over the hemispheric grid, configured to support the CAMx cloud-in-grid (CiG) convective sub-model and to test H-CAMx sensitivity to improved vertical resolution in the mid-troposphere through lower stratosphere that is similar to GOES-Chem;
- Expand the H-CAMx application to the entire year of 2016, extend the model performance evaluation to include additional global surface and upper air measurement data for ozone, particulate matter and key precursors, and compare evaluation results to 2016 applications of the GEOS-Chem global model and EPA's H-CMAQ;
- Apply OSAT over the entire year of 2016, tracking boundary contributions separately to differentiate stratospheric ozone intrusion versus near-equatorial contributions, and apply the Particulate Source Apportionment Tool (PSAT) to investigate transport of Saharan dust and Central American fire smoke into Texas;
- Identify and implement updates that enhance model speed, such as selecting the EQSAM inorganic particulate chemistry as an alternative to ISORROPIA, developing a compact version of the CB6 chemistry mechanism with fewer species and reactions, and incorporating a faster chemistry solver;
- After updates above during FY2020, integrate H-CAMx into the Near Real Time Exceptional Event Modeling (NRTEEM) system during FY2021, including hemispheric ozone and particulate source apportionment to provide expanded daily global impact assessments.

6.0 REFERENCES

Astitha et al., 2012. Parameterization of dust emissions in the global atmospheric chemistry-climate model EMAC: impact of nudging and soil properties. *Atmos. Chem. Phys.*, 12(22):11057-11083, doi:10.5194/acp-12-11057-2012.

Bey, I., D.J. Jacob, R.M. Yantosca, J.A. Logan, B.D. Field, A.M. Fiore, Q. Li, H.Y. Liu, L.J. Mickley, M.G. Schultz, 2001. Global modeling of tropospheric chemistry with assimilated meteorology: Model description and evaluation. *J. Geophys. Res. Atmos.*, 106(D19), 23073–23095, 2001.

CEDS, 2019. Joint Global Change Research Institute CEDS website: http://www.globalchange.umd.edu/ceds/

Eastham, S.D. and D.J. Jacob, 2017. Limits on the ability of global Eulerian models to resolve intercontinental transport of chemical plumes. *Atmos. Chem. Phys*., 17(4), 2543–2553, doi:10.5194/acp-17-2543-2017, 2017.

EDGAR, 2019. Hemispheric Transport of Air Pollutants (HTAP v2) emission inventory website: http://edgar.jrc.ec.europa.eu/htap_v2/

Emery, C. and G. Yarwood, 2019. Modeling Protocol: Development and Testing of a Hemispheric Comprehensive Air Quality Model with Extensions (CAMx) Application Scoping Study for Development/Application of CAMx for the Northern Hemisphere (Work Order No. 582-19-93346-05). Prepared for the Texas Commission on Environmental Quality, Austin, TX. Prepared by Ramboll, Novato, CA (February 2019).

EPA, 2018. Global-scale Simulation Model Operational Evaluation Protocol. U.S. Environmental Protection Agency, Office of Air Quality Planning and Standards, Air Quality Assessment Division, Research Triangle Park, NC (March 1, 2018).

EPA, 2019. Biogenic Emission Inventory System (BEIS) website: https://www.epa.gov/air-emissions-modeling/biogenic-emission-inventory-system-beis

GEIA, 2019. Global Emissions Initiative (GEIA) website: http://www.igacproject.org/activities/GEIA

Gong, S.L. 2003. A parameterization for sea-salt aerosol source function for sub- and super-micron particle sizes. *Biogeochemical Cycles*, 17, 1097-1104.

Harvard University, 2019. GEOS-Chem Model website. http://acmg.seas.harvard.edu/geos

Klingmueller et al, 2017. Revised mineral dust emissions in the atmospheric chemistry-climate model EMAC (based on MESSy 2.52). *Geosci. Model Dev. Discuss*., https://doi.org/10.5194/gmd-2017-160

Kondo, J., 1975. Air-sea bulk transfer coefficients in diabatic conditions. *J. Meteorol*., 9, 91–112.

Lana, A., et al., 2011. An updated climatology of surface dimethlysulfide concentrations and emission fluxes in the global ocean. *Global Biogeochem. Cycles*, 25, GB1004, doi:10.1029/2010GB003850, http://onlinelibrary.wiley.com/do/10.1029/2010GB003850/full

Liss, P., and L. Merlivat. 1986. Air-sea gas exchange rates: Introduction and synthesis, in *The Role of Air-Sea Exchange in Geochemical Cycling*, edited by P. Buat-Ménard, pp. 113–128, D. Reidel, Dordrecht, Netherlands.

Mathur, R., J. Xing, R. Gilliam, G. Sarwar, C. Hogrefe, J. Pleim, G. Pouliot, S. Roselle, T.L. Spero, D.C. Wong, J. Young, 2017. Extending the Community Multiscale Air Quality (CMAQ) modeling system to hemispheric scales: overview of process considerations and initial applications. *Atmos. Chem. Phys*., 17, 12449–12474.

McGillis, W.R., Dacey, J.W.H., Frew, N.M., Bock, E.J., Nelson, R.K., 2000. Water-air flux of dimethylsulfide. J*. Geophys. Res*., 105(C1), 1187–1193.

NCAR, 2019a. Fire Inventory from NCAR web site: https://www2.acom.ucar.edu/modeling/finn-fire-inventory-ncar

NCAR, 2019b. Model of Emissions of Gases and Aerosols from Nature (MEGAN) website: https://www2.acom.ucar.edu/modeling/model-emissions-gases-and-aerosols-nature-megan

Nightingale, P.D., Malin, G., Law, C.S., Watson, A.J., Liss, P.S. Liddicoat, M.I., Boutin, J., Upstill-Goddard, R.C., 2000. In situ evaluation of air-sea gas exchange parameterizations using novel conservative and volatile tracers. *Global Biogeochem. Cycles*, 14(1), 373–387.

Nopmongcol, U., M. Zatko, R. Morris. 2019. International Contributions to Regional Haze: Global Chemical Transport Model Methodology and Results. Prepared for the Electric Power Research Institute, Palo Alto, CA; by Ramboll, Novato, CA (January, 2019).

Ovadnevaite, J., et al. 2014. A sea spray aerosol flux parameterization encapsulating wave state. *Atmos. Chem. Phys*., 14, 1837-1852.

Ramboll. 2019. Global Observation Dataset Selection for GEOS-Chem Model Performance Evaluation (Work Order No. 82-19-92775-04). Prepared for the Texas Commission on Environmental Quality, Austin, TX. Prepared by Ramboll, Novato, CA (April 2019).

Saltzman, E.S., King, D.B., Holmen, K., Leck, C., 1993. Experimental determination of the diffusion coefficient of Dimethylsulfide in water. *J. Geophys. Res*., 98(C9), 16,481–16,486.

Skamarock, W.C., Klemp, J.B., Dudhia, J., Gill, D.O., Barker, D.M., Dudha, M.G., Huang, X., Wang, W., Powers, Y., 2008. A description of the advanced research WRF Ver. 30. NCAR Technical Note (p. 113). NCAR/TN-475.

WMO. 1992. *International Meteorological Vocabulary* (2nd ed.), Geneva: Secretariat of the World Meteorological Organization. p. 636. ISBN 978-92-63-02182-3.

Xing, J., R. Mathur, J. Pleim, C. Hogrefe, J. Wang, C.-M. Gan, G. Sarwar, D.C. Wong, S. McKeen, 2016. Representing the effects of stratosphere–troposphere exchange on 3-D O_3 distributions in chemistry transport models using a potential vorticity-based parameterization. *Atmos. Chem. Phys*., 16, 10865–10877, doi:10.5194/acp-16-10865-2016.

Zhuang, J., D.J. Jacob, S.D. Eastham, 2017. The importance of vertical resolution in the free troposphere for modeling intercontinental plumes. *Atmos. Chem. Phys. Discuss*., https://doi.org/10.5194/acp-2017-1124